JCB Journal of Cell Biology

ARTICLE

Centrosome amplification disrupts renal development and causes cystogenesis

Lai Kuan Dionne[1*], Kyuhwan Shim[1*], Masato Hoshi[1], Tao Cheng[1], Jinzhi Wang[1], Veronique Marthiens[3], Amanda Knoten[1], Renata Basto[3], Sanjay Jain[1,4], and Moe R. Mahjoub[1,2]

Centrosome number is tightly controlled to ensure proper ciliogenesis, mitotic spindle assembly, and cellular homeostasis. Centrosome amplification (the formation of excess centrosomes) has been noted in renal cells of patients and animal models of various types of cystic kidney disease. Whether this defect plays a causal role in cystogenesis remains unknown. Here, we investigate the consequences of centrosome amplification during kidney development, homeostasis, and after injury. Increasing centrosome number in vivo perturbed proliferation and differentiation of renal progenitors, resulting in defective branching morphogenesis and renal hypoplasia. Centrosome amplification disrupted mitotic spindle morphology, ciliary assembly, and signaling pathways essential for the function of renal progenitors, highlighting the mechanisms underlying the developmental defects. Importantly, centrosome amplification was sufficient to induce rapid cystogenesis shortly after birth. Finally, we discovered that centrosome amplification sensitized kidneys in adult mice, causing cystogenesis after ischemic renal injury. Our study defines a new mechanism underlying the pathogenesis of renal cystogenesis, and identifies a potentially new cellular target for therapy.

Introduction

The centrosome and associated primary cilium act together as a cellular hub to regulate several important developmental signaling pathways (Bettencourt-Dias et al., 2011; Arquint et al., 2014). Most quiescent cells in the human body contain a solitary centrosome and cilium. As cells proliferate, the number of centrosomes is tightly regulated via a duplication and segregation mechanism linked to the cell cycle (Nigg and Stearns, 2011; Brito et al., 2012). Dysregulation of centrosome biogenesis can result in the formation of extra centrosomes in a cell, a phenomenon termed centrosome amplification (CA). Although CA is rare in healthy tissues, the presence of supernumerary centrosomes has been noted in malignant lesions and correlates with increased tumor grade, size, and metastasis of various types of cancer (Krämer et al., 2005; Nigg, 2006; Godinho et al., 2009; Godinho and Pellman, 2014; Cosenza and Kramer, 2016; Nano and Basto, 2016). The presence of CA in tumors has raised the question of whether they are innocent bystanders or play a causative role in tumorigenesis. Extensive studies in vivo have thus far yielded variable results. For example, induction of CA in the skin of mice failed to promote formation of tumors (Kulukian et al., 2015; Vitre et al., 2015). Similarly, CA in mouse embryonic brain neural stem cells results in aneuploidy, cell death, and microcephaly, but not tumorigenesis (Marthiens et al., 2013). In contrast, CA can initiate spontaneous formation of lymphomas and squamous cell carcinomas in aged mice in the presence (Levine et al., 2017) or absence of p53 (Serçin et al., 2016).

Although most studies have focused on the role of CA in genome instability and cancer, little is known about its impact on ciliary function. This is surprising, because the centrosome provides the structural support for cilium formation, coordinates ciliary protein trafficking, and thus modulates ciliary signaling (Bettencourt-Dias et al., 2011; Arquint et al., 2014). To address this gap in knowledge, we previously tested the effects of CA on ciliary assembly and signaling in vitro. We induced CA by briefly overexpressing Polo-like kinase 4 (Plk4), known as the master regulator of centrosome duplication, which causes formation of supernumerary centrosomes in a diversity of cells and organisms (Habedanck et al., 2005; Sillibourne and Bornens, 2010). Remarkably, we discovered that CA disrupted ciliogenesis, resulting in cells that either lacked cilia (aciliated) or formed more than one cilium (superciliated; Mahjoub and Stearns, 2012). Both ciliogenesis defects led to aberrant ligand-dependent ciliary signaling, and subsequently disrupted ciliary-dependent cellular processes (Mahjoub and Stearns, 2012). Together, these data

[1]Division of Nephrology, Department of Medicine, Washington University School of Medicine, St. Louis, MO; [2]Department of Cell Biology and Physiology, Washington University School of Medicine, St. Louis, MO; [3]Centre National de la Recherche Scientifique—Institute Curie, Paris, France; [4]Department of Pathology and Immunology, Washington University School of Medicine, St. Louis, MO.

*L.K. Dionne and K. Shim contributed equally to this paper; Correspondence to Moe R. Mahjoub: mmahjoub@wustl.edu.

https://doi.org/10.1083/jcb.201710019

indicate that CA has a detrimental effect on ciliary signaling and function. Based on these observations, we hypothesized that CA might play a prominent role in the pathogenesis of ciliopathies, the etiology of which is ciliary dysfunction.

In support of this theory, CA was recently noted in kidneys of patients and animal models of various types of cystic kidney disease, a well-established ciliopathy. For example, loss of the genes responsible for causing autosomal-dominant polycystic kidney disease (ADPKD), *PKD1* and *PKD2*, induced CA in renal cells in vitro, whereas CA was observed in kidneys of knockout mice and patients in vivo (Battini et al., 2008; Burtey et al., 2008). Mutations in the ciliary protein Inversin causes nephronophthisis, an autosomal-recessive form of cystic kidney disease (Simons et al., 2005; Srivastava et al., 2018). Loss of Inversin in the developing mouse nephron also leads to an increased frequency of cells that contain extra centrosomes in vivo (Werner et al., 2013). Deletion of the centrosomal Mks1 or Mks3 proteins, mutated in Meckel-Gruber syndrome patients who present with cystic kidneys, similarly results in CA in renal cells (Tammachote et al., 2009). Loss of the tumor suppressor genes *TSC1* and *TSC2*, mutations that cause tuberous sclerosis and renal cystogenesis, also lead to CA (Astrinidis et al., 2006; Hartman et al., 2009). Similarly, CA has been observed in kidney epithelia after mutations in other ciliary and centrosomal genes that cause cystic kidney disease (Jonassen et al., 2008; Chen et al., 2014). Collectively, these results indicate that CA may be a common feature of renal cystogenesis and suggest that regardless of the cyst-inducing mutation, CA itself may be a cellular defect that helps to promote or drive cystogenesis. Surprisingly, this theory has remained untested.

In this study, we examined the consequences of CA in the developing embryonic mammalian kidney, and during adult kidney homeostasis. We discovered that increasing centrosome number in vivo disrupted renal progenitor cell proliferation and differentiation, resulting in defective branching morphogenesis and renal hypoplasia at birth. CA caused abnormal mitotic spindle assembly and disrupted ciliary assembly and signaling, highlighting the mechanisms underlying the observed cellular and developmental defects. Remarkably, CA induced rapid cyst growth and expansion postnatally. In contrast, induction of CA in differentiated nephron epithelia of mature kidneys caused ciliogenesis defects, but not cyst formation, highlighting intrinsic differences between proliferating and quiescent cells. Finally, we found that CA sensitized kidneys in adult mice, causing cystogenesis after ischemic renal injury. Together, our results demonstrate that CA is detrimental to renal development and is sufficient to trigger cyst formation in the absence of cystic gene mutations.

Results

Mouse models of CA in the developing embryonic kidney

The mammalian kidney develops via reciprocal signaling between two distinct progenitor compartments, the ureteric bud epithelium (UB) and metanephric mesenchyme (MM; Fig. 1 A). MM cells adjacent to UB branch tips are induced to form the epithelia of the glomerulus, proximal and distal tubules of mature nephrons. In turn, the UB is stimulated by MM to undergo successive branching events to form collecting ducts (a process termed renal branching morphogenesis; Hendry et al., 2011). Disruption of reciprocal signaling between the UB and the MM during branching morphogenesis has detrimental effects on the overall proliferation and differentiation of both populations of progenitors and kidney development (Hendry et al., 2011). To induce CA in a spatiotemporally controlled manner, we used a mouse model that we recently developed with which overexpression of mCherry-tagged Plk4 (mChPlk4) can be induced by cell type-specific Cre-recombinase expression (Marthiens et al., 2013; Fig. 1 A and Fig. S1). To cause CA in the UB, we bred mChPlk4 mice to a Hoxb7-Cre (Zhao et al., 2004) strain that expresses Cre in the UB lineage (hereafter named Hoxb7-Plk4). To induce CA in the MM, mChPlk4 mice were crossed with the Six2-Cre (Kobayashi et al., 2008) strain that express Cre-recombinase in the MM lineage (hereafter called Six2-Plk4; Fig. 1 A and Fig. S1). We examined kidneys from both crosses at various stages of embryonic development (embryonic day [E] 13.5, E15.5, and E17.5) and postnatally (postnatal day [P] 0, P7, and P15). The number of animals analyzed from each genotype is summarized in Table S1.

We confirmed the specificity of Plk4 expression by staining kidney sections with antibodies against mCherry. As expected, mChPlk4 expression in Hoxb7-Plk4 mice at E13.5 was restricted to E-cadherin–positive UB epithelia and was absent from Six2-positive MM, or their derivative structures marked by WT1 (Mundlos et al., 1993; Fig. S2). Similarly, mChPlk4 expression in Six2-Plk4 animals was restricted to the Six2- and WT1-positive cells, but not UB epithelia (Fig. S2). Importantly, no mChPlk4 expression was evident in control littermates containing only one of the two transgenes (Fig. S2). This cell type–specific expression persisted throughout embryonic development from E15.5 to E17.5 (Figs. S3 and S4). Next, we investigated the effect of mChPlk4 expression on centrosome number in the two progenitor populations. Centrosome number was quantified by immunostaining with antibodies specific for γ-tubulin, a core component of the centrosome (Nigg and Stearns, 2011; Brito et al., 2012; Goto et al., 2013). In Hoxb7-Plk4 embryos, we observed an increase in centrosome number, specifically in UB cells overexpressing mChPlk4, whereas centrosome number appeared normal in neighboring tubular cells lacking mChPlk4, and in kidneys of control littermates (Fig. 1, B and C; and Fig. S5, A and B). Similarly, CA was evident in the MM of Six2-Plk4 embryos specifically in cells overexpressing Plk4 (Fig. 1, B and C; and Fig. S5, A and B). Quantification of CA showed that roughly 60% of UB cells contained more than two centrosomes per cell, whereas ∼40% of MM contained excess centrosomes at E15.5 to E17.5 (Fig. 1, B and C; and Fig. S5, A and B).

CA impairs embryonic kidney development

Analysis of Hoxb7-Plk4 and Six2-Plk4 embryos revealed a significant reduction in kidney size compared with control animals (Fig. 2 A). To determine why these kidneys were small, we measured changes in the abundance of nephrogenic precursors over time. Quantification of Six2-positive and total MM cells per mesenchymal cap structure revealed a large decrease in the overall cell population at E15.5 to E17.5 compared with control kidneys (Fig. 2, B–D; and Fig. S5 C). This decrease was observed in both Hoxb7-Plk4 and Six2-Plk4 embryos. Because Six2-Cre transgenic

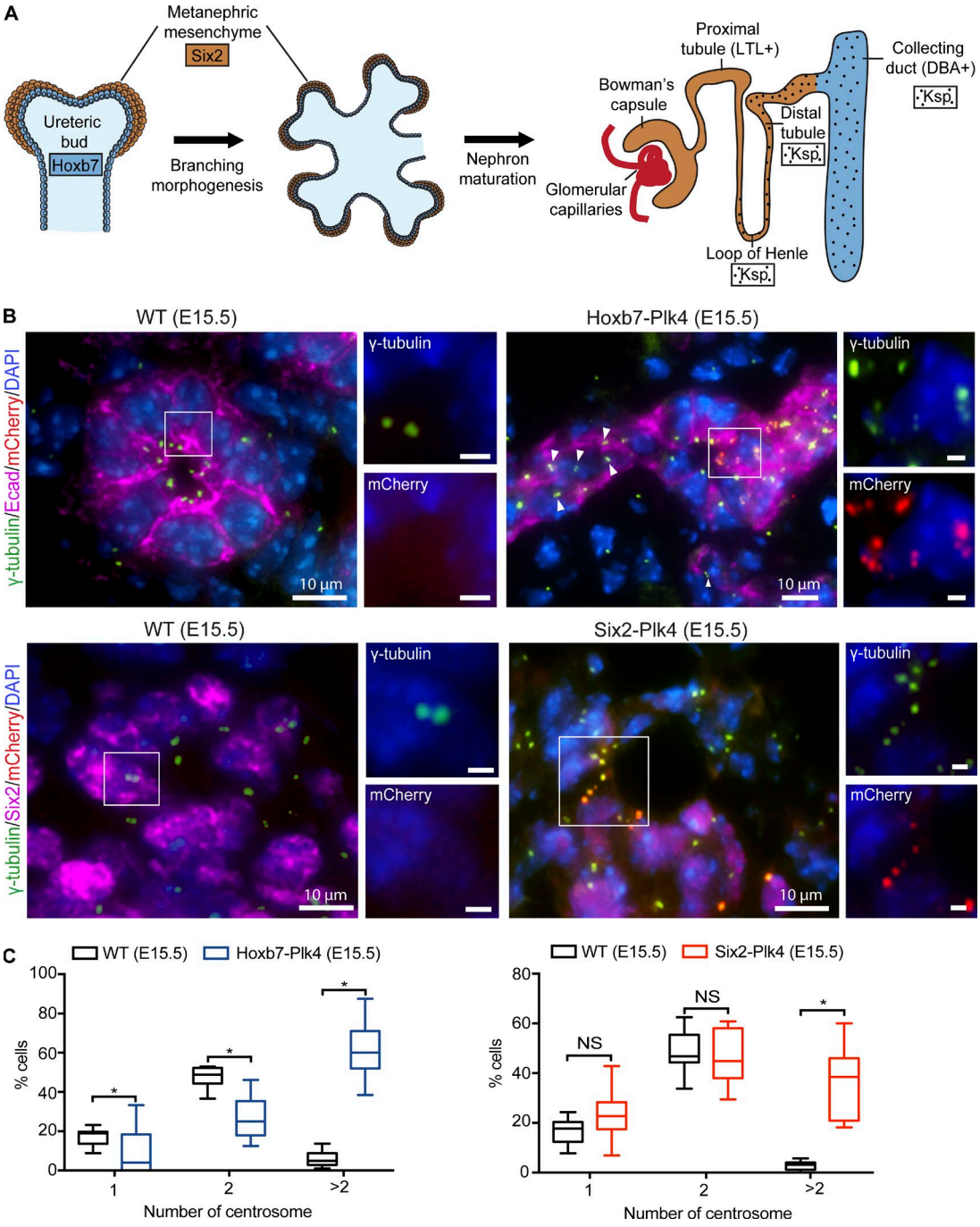

Figure 1. **Conditional Plk4 expression and CA in the developing mouse kidney. (A)** Schematic representation of nephrogenesis, from renal progenitors to mature nephrons. Diagram highlights the progenitor cell type and nephron segment-specific expression of Plk4 mediated by Six2-Cre (brown), Hoxb7-Cre (blue), and Ksp-Cre (dots). **(B)** Kidney sections from E15.5 control, Hoxb7-Plk4 (top), and Six2-Plk4 (bottom) mice were immunostained with antibodies targeting mCherry (Plk4), γ-tubulin (centrosomes), E-cadherin (UB tubules), or Six2 (MM). Control kidneys lacking mChPlk4 mainly contain one centrosome with one to two foci. In Hoxb7-Plk4, excess centrosomes are seen specifically in regions of UB tubules overexpressing mChPlk4 (white box, magnified 1.5-fold). Importantly, adjacent cells within the same tubule that lack mChPlk4 signal display normal centrosome doublets (arrowheads). Nuclei were stained with DAPI. Similarly, supernumerary centrosomes were seen specifically in cells overexpressing mChPlk4 in Six2-Plk4 mice (white box, magnified 1.5-fold). Nuclei were stained with DAPI. Bars (insets), 2 µm. **(C)** Graphs show the percentage of cells with normal centrosome number (one or two) or CA (more than two centrosomes) in Hoxb7-Plk4 or Six2-Plk4 mice. Centrosome number was quantified per nucleus of the cells in each progenitor population, using cell-specific markers (E-cadherin or Six2). n = 1,210 cells (E15.5 WT control), 324 mChPlk4-positive cells (E15.5 Hoxb7-Plk4), 1,442 cells (E15.5 WT control), and 277 mChPlk4-positive cells (E15.5 Six2-Plk4). Box plots represent the median, maximum, and minimum values for each dataset. A two-tailed unpaired t test was performed to determine statistically significant differences between samples (*, $P < 0.05$).

animals coexpress GFP in the MM, we visualized dynamic changes in the density of MM during branching morphogenesis, using a metanephric explant culture system (Keefe Davis et al., 2013). Kidneys from Six2-Cre^{GFP} or Six2-Cre^{GFP}-Plk4 embryos were isolated at E13.5 and cultured ex vivo, and the density of the MM was visualized for 36 h using live-cell imaging. We noted a progressive decrease in the density of MM per cap as branching morphogenesis proceeded (Fig. 2 E and Video 1), consistent with the decrease observed in vivo (Fig. 2, B–D). Similarly, analysis of early UB branching of Hoxb7-Cre^{GFP} and Hoxb7-Cre^{GFP}-Plk4 embryos showed a decrease in branching morphogenesis over time, resulting in more than 50% reduction of ureteric bud tips at 36 h (Fig. 2, E and F; and Video 2). Finally, we tested whether CA disrupted the differentiation potential of MM cells into glomerular precursor structures, characterized by expression of the transcription factor WT1 (Mundlos et al., 1993). We discovered a significant decrease in WT1-positive structures in Hoxb7-Plk4 and Six2-Plk4 embryos from E15.5 to E17.5 (Fig. 2, B and G; and Fig. S5 C), highlighting a differentiation defect of progenitors upon CA.

To further elucidate the cause of the nephrogenesis defects, we quantified the proliferation indices of renal progenitors over time. There was a significant decrease in phospho-histone H3 (pHH3)–positive mitotic cells per unit area of E15.5 Hoxb7-Plk4 and Six2-Plk4 kidneys compared with controls (Fig. 3, A and B). Intriguingly, there was no difference in proliferation rates between E17.5 and P0 (Fig. 3, A and B), which suggests that the detrimental effects of CA on progenitor cell proliferation occur only during very early stages of nephrogenesis. Next, we determined whether the reduction in the progenitor population was a result of increased apoptosis, as CA in various tissues causes cell death (Marthiens et al., 2013; Coelho et al., 2015; Kulukian et al., 2015; Serçin et al., 2016; Levine et al., 2017). Indeed, the number of apoptotic nuclei per unit area, identified using the TUNEL assay, was significantly increased in the UB and MM cells of Hoxb7-Plk4 and Six2-Plk4 kidneys at E15.5 to E17.5 (Fig. 3, C and D). Reduction in progenitor number during early kidney development can limit the number of cells available for nephrogenesis, resulting in smaller kidneys because of reduced nephron endowment (Hendry et al., 2011). Consistent with these findings, kidneys of Hoxb7-Plk4 and Six2-Plk4 animals were significantly smaller at birth compared with control littermates (Fig. 3, E and F). To determine whether the reduction in overall kidney size was cause by decreased nephron number, we quantified the number of glomeruli. Indeed, there was a large decrease in the mean number of glomeruli in Hoxb7-Plk4 and Six2-Plk4 animals (Fig. 3, G and H). Collectively, these analyses of cell proliferation, differentiation, apoptosis, and branching morphogenesis indicate that CA interferes with the growth and survival of nephrogenic progenitors, decreasing the size of the pool available for nephron formation.

CA disrupts ciliogenesis and mitotic spindle morphology

We sought to determine the cellular and molecular defects underlying the reduced proliferation and differentiation of the renal progenitor population. We reasoned that CA may result in aberrant ciliary assembly and signaling, similar to what we observed in vitro (Mahjoub and Stearns, 2012). Cilia play an important role in renal progenitor cell growth and survival (Chi et al., 2013). Genetic ablation of cilia in the MM or UB of embryonic mouse kidneys disrupts signaling pathways that are critical for proliferation and differentiation of both progenitor pools (Chi et al., 2013). To test whether CA disrupted ciliogenesis in the two progenitor populations, we immunostained kidneys from E15.5 to E17.5 Hoxb7-Plk4 and Six2-Plk4 animals for centrosomes and cilia. There was an increase in aciliated and superciliated cells in the UB and MM of these mice, respectively (Fig. 4, A and B; and Fig. S5 D). This corresponded with a decrease in the fraction of cells containing the normal complement of one cilium. In contrast, the majority of cells containing normal centrosome numbers assembled one cilium, indicating that the observed ciliary defects are specific to cells with CA (Fig. 4, A and B; and Fig. S5 D).

Genetic ablation of cilia in embryonic kidneys disrupts signaling pathways essential for progenitor cell expansion (Chi et al., 2013), including the WNT11/RET-ERK signaling cascade needed for UB branching morphogenesis (Fisher et al., 2001; Majumdar et al., 2003), and the WNT4-LEF1 pathway necessary for the maintenance and differentiation of the MM population (Schmidt-Ott and Barasch, 2008; Mugford et al., 2009; Brown et al., 2013). We wondered whether induction of CA, which disrupts ciliogenesis (Fig. 4, A and B), was similarly attenuating these signaling pathways. Immunostaining of kidney sections from E15.5 Hoxb7-Plk4 showed a significant reduction in WNT11 and RET levels in UB tubules (Fig. 4, C and D). RET activates downstream signaling pathways including ERK/MAPK, which helps regulate UB cell proliferation and renewal (Jain, 2009). We noted a large reduction in phosphorylated ERK in kidneys of E15.5 mice (Fig. 4, C and D), indicating that the RET-MAPK pathway was disrupted. Similarly, there was a significant decrease in the number of LEF1-positive cells in renal vesicles of E15.5 animals (Fig. 4, C and D), suggesting that WNT4-dependent growth/differentiation of the MM was attenuated. Thus, CA abrogates signaling pathways essential for UB and MM progenitor cell growth and differentiation by disrupting ciliary assembly.

CA is also known to cause defects in mitotic spindle assembly by promoting the formation of multipolar or pseudobipolar spindles leading to chromosome missegregation, aneuploidy, and cell death (Ganem et al., 2009; Silkworth et al., 2009; Janssen et al., 2011; Ogden et al., 2013; Godinho et al., 2014). Thus, we characterized the morphology of the mitotic spindle in dividing progenitors at various developmental stages. All mitotic cells of control animals consistently formed normal, bipolar spindles between E15.5 and E17.5 (Fig. 4, E and F). Moreover, as these cells differentiated into mature nephrons between P0 and P15, they continued to exclusively form bipolar spindles. In contrast, a significant number of cells with CA formed multipolar spindle configurations at E15.5 (Fig. 4, E and F). The high incidence of multipolar spindles at E15.5 correlated with the decrease in cell proliferation and increased cell death observed at that developmental stage (Fig. 3, A–D). However, the fraction of cells with multipolar mitoses decreased dramatically as renal development proceeded (Fig. 4, E and F). A mechanism known as "centrosome clustering" helps promote the focusing of extra centrosomes into two main poles during late metaphase, to ensure bipolar segregation of chromosomes and thus

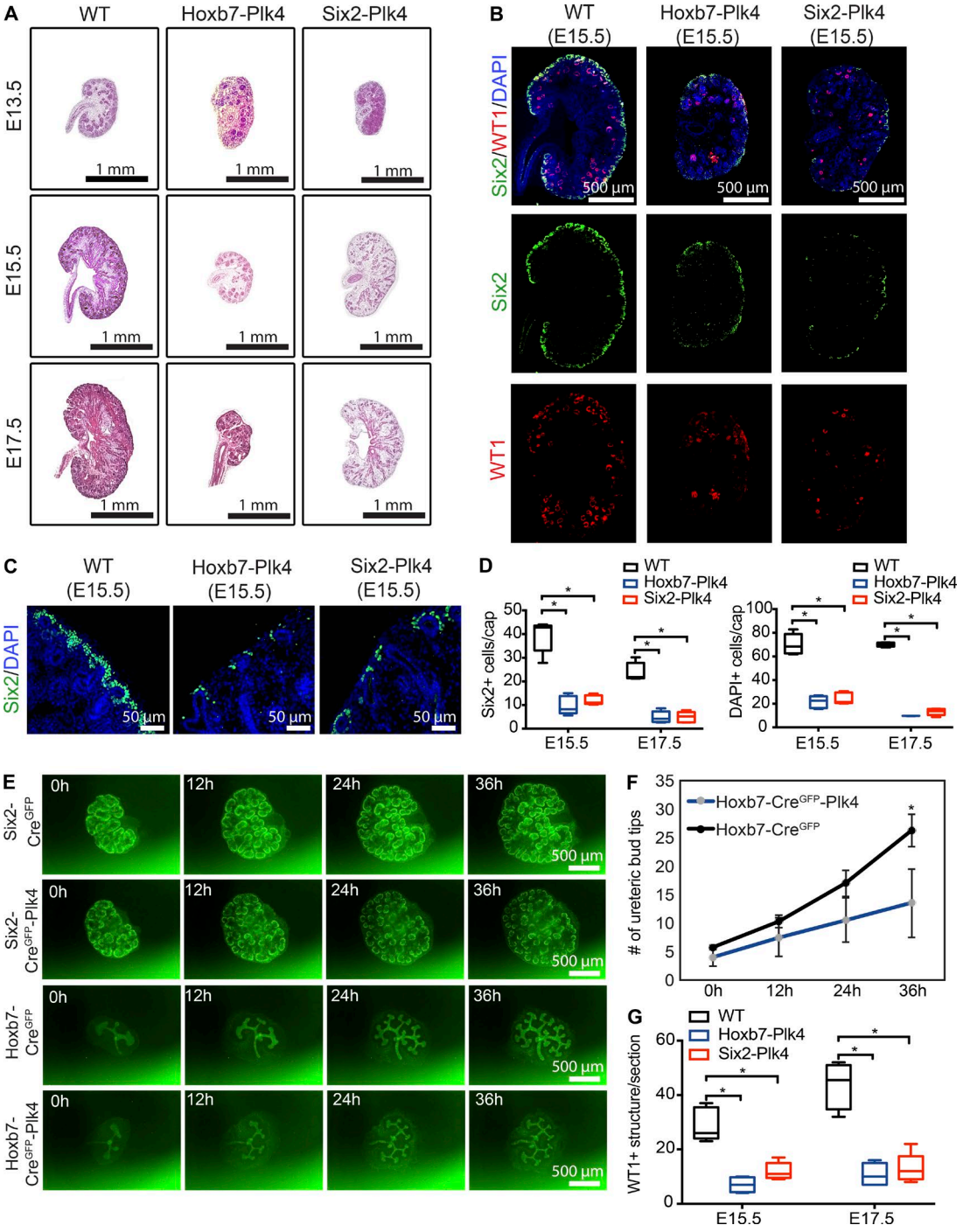

Figure 2. **CA impairs embryonic renal development. (A)** H&E staining of kidney sections from E13.5 to E17.5 Hoxb7-Plk4, Six2-Plk4, and control embryos. **(B)** Immunofluorescence images of kidney sections from E15.5 mice stained with antibodies against Six2 (to identify MM cells) and WT1 (glomerular precursors). Nuclei are stained with DAPI. There was a significant decrease in the density of both Six2-positive progenitors and WT1-positive structures compared with control samples. **(C)** Higher magnification images of the distribution of Six2-positive MM cells in Hoxb7-Plk4, Six2-Plk4, and control embryos at E15.5, highlighting the reduced concentration of mesenchymal progenitors. **(D)** Quantification of the number of Six2-positive progenitors and total MM cell density (DAPI-positive nuclei) per UB tip structure from E15.5 to E17.5. Data represent 25 UB tip structures scored from five mice of each genotype at each time point. Two-tailed unpaired *t* test was used for statistical analysis (*, $P < 0.05$). **(E)** Representative images from live-cell imaging of kidney explant cultures of Six2-Cre^{GFP}-Plk4, Hoxb7-Cre^{GFP}-Plk4, and relevant controls. We note a progressive decrease in the density of the MM in Six2-Cre^{GFP}-Plk4 kidneys, and reduced number of ureteric branches in Hoxb7-Cre^{GFP}-Plk4 compared with control mice. **(F)** Quantification of the number of UB tips in Hoxb7-Cre^{GFP}-Plk4 and control kidneys, as shown in E. $n = 4$ kidneys analyzed for each genotype. A two-tailed unpaired *t* test was used for statistical analysis (*, $P < 0.05$). Error bars denote SD. **(G)** Quantification of the number of WT1-positive structures per kidney section from E15.5 to E17.5, examples of which are shown in B. $n = 5$ kidneys analyzed for each genotype (E15.5), and $n = 4$ for each genotype (E17.5). A two-tailed unpaired *t* test was used for statistical analysis (*, $P < 0.05$).

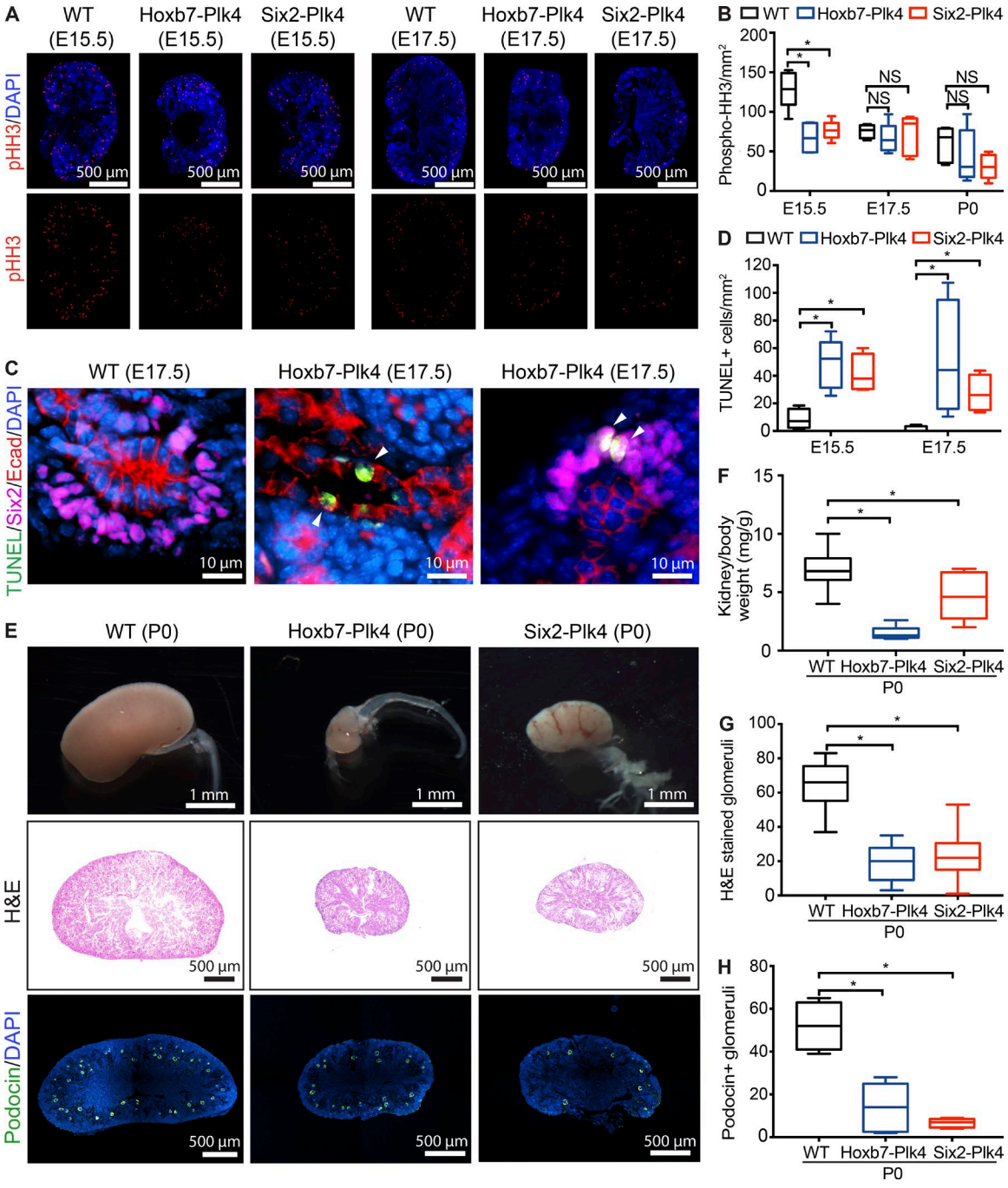

Figure 3. **CA results in decreased cell proliferation, increased apoptosis, and reduced nephron endowment. (A)** E15.5 and E17.5 kidney sections immunostained with anti-pHH3 to mark proliferating mitotic cells. Nuclei were stained with DAPI. **(B)** Quantification of pHH3-positive mitotic cells per unit area (mm^2) in kidney sections from Hoxb7-Plk4, Six2-Plk4, and control embryos at E15.5, E17.5, and P0. There was a significant decrease in pHH3 foci/mm^2 predominantly at E15.5, with no statistically significant differences at later time points. A minimum of four to five sections was scored per genotype at each developmental stage. A two-tailed unpaired *t* test was used for statistical analysis (*, $P < 0.05$). **(C)** Representative images from E17.5 Hoxb7-Plk4 and control mice stained for apoptotic cells (TUNEL), E-cadherin (UB tubules), and Six2 (MM). Nuclei were stained with DAPI. Apoptotic cells (white arrowheads) were evident in both UB and MM cells. **(D)** Graph illustrating the fraction of TUNEL-positive cells per unit area (mm^2) in kidneys between E15.5 and E17.5. $n = 5$ kidneys per genotype for each time point. Statistical significance was determined using a two-tailed unpaired *t* test (*, $P < 0.05$). **(E)** Brightfield image of whole kidneys (top) and H&E staining of midsagittal sections (middle) from Hoxb7-Plk4, Six2-Plk4, and control littermates at P0, highlighting the small kidney phenotype at birth. Immunofluorescence images (bottom) of sections stained for Podocin to identify glomeruli. Nuclei were stained with DAPI. **(F)** Quantification of kidney–to–body weight ratio, highlighting a significant reduction in kidney size. $n = 33$ (WT), 7 (Hoxb7-Plk4), and 5 (Six2-Plk4). **(G and H)** Quantification of the mean number of glomeruli per section from H&E- (G) and Podocin-stained (H) sections. There was a significant decrease in the number of glomeruli in Hoxb7-Plk4 and Six2-Plk4 mice compared with control, indicative of reduced nephron endowment. $n = 7$ (WT) and 5 (Hoxb7-Plk4 and Six2-Plk4). Two-tailed unpaired *t* test was used for statistical analysis (*, $P < 0.05$).

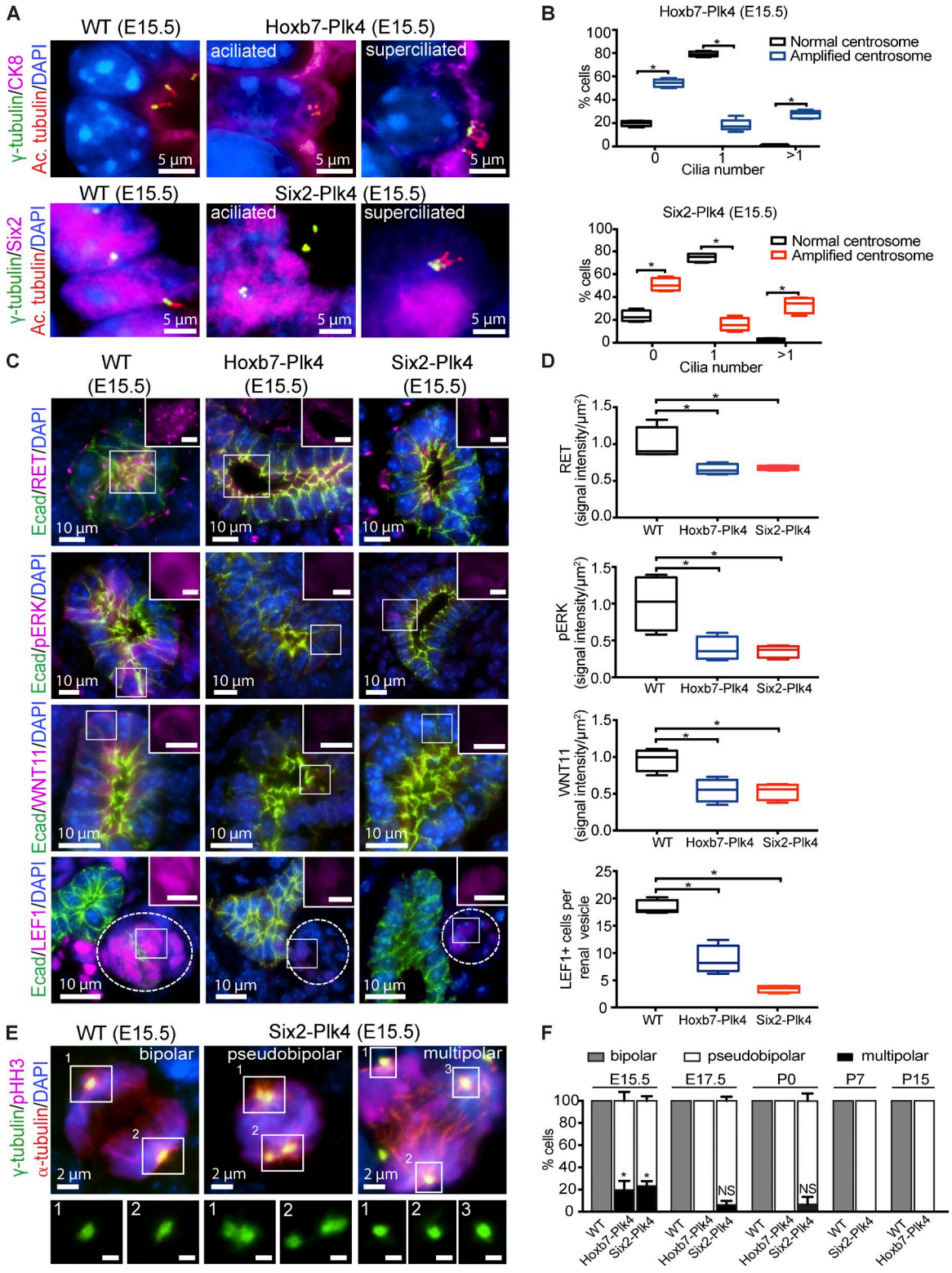

Figure 4. **CA disrupts ciliogenesis and mitotic spindle morphology. (A)** Immunostaining of E15.5 kidney sections from Hoxb7-Plk4, Six2-Plk4, and control embryos with antibodies against γ-tubulin (centrosomes), acetylated α-tubulin (cilia; Ac. tubulin), CK8 (UB epithelia), Six2 (MM), and DAPI (DNA). Normal kidney cells contain one centrosome and cilium, whereas progenitor cells with excess centrosomes are either aciliated or superciliated. **(B)** Quantification of ciliary assembly defects in UB cells of Hoxb7-Plk4 mice or MM cells of Six2-Plk4 mice. The percentage of cells with zero, one, or more than one cilium was determined from cells that contained normal centrosome number compared with cells with CA. *n* = 311 cells (E15.5 WT control; normal centrosomes), 263 cells (E15.5 Hoxb7-Plk4; amplified centrosomes), 253 cells (E15.5 WT control; normal centrosomes), and 238 cells (E15.5 Six2-Plk4; amplified centrosomes) from five mice of each genotype per developmental stage. Statistical significance was determined by a two-tailed unpaired *t* test (*, $P < 0.05$). **(C)** Representative images from E15.5 kidney sections of control, Hoxb7-Plk4, and Six2-Plk4 embryos immunostained with antibodies against RET, phospho-ERK, WNT11, LEF1, E-cadherin, and DAPI. Bars (insets), 5 μm. **(D)** Graphs showing relative levels of RET, pERK, and WNT11 in ureteric buds of E15.5 WT, Hoxb7-Plk4, or Six2-Plk4 mice. The

survival of cells with CA (Quintyne et al., 2005; Marthiens et al., 2012). We found that cells with CA predominantly clustered their centrosomes into a pseudobipolar configuration after E15.5 (Fig. 4, E and F). Collectively, these results suggest that CA-induced defects in ciliary assembly/function and mitotic spindle morphology underlie reduced progenitor cell proliferation, reduced differentiation, and increased cell death, and are likely the main causes of kidney size reduction observed in Hoxb7-Plk4 and Six2-Plk4 embryos.

CA causes cystogenesis

Defects in primary cilia assembly or function are a root cause of cystogenesis in various renal cystic diseases (Yoder, 2007; Sharma et al., 2008; Ma et al., 2017). Ablation of cilia in the mouse kidney during gestation results in severely cystic kidneys shortly after birth (Lin et al., 2003; Davenport et al., 2007). Because CA resulted in defective ciliogenesis in Hoxb7-Plk4 and Six2-Plk4 mice (Fig. 4, A and B), we hypothesized that these animals would develop cysts over time. Indeed, CA resulted in rapid-onset cystogenesis in both mouse models by P15 (Fig. 5 A). Although the kidneys were still smaller than control animals (because they were small since birth), both models developed large fluid-filled cysts. Although these mice were born in the expected Mendelian ratios, most died by P15 (Table S1) which was particularly evident for Six2-Plk4. Thus, we focused the subsequent analyses of Six2-Plk4 at P7 (Fig. S6 A).

To determine whether CA and ciliogenesis defects persisted in cystic epithelia, we immunostained P7 and P15 sections for centrosomes and cilia. Consistent with our genetic scheme, we saw a modest but significant amount of CA in cystic epithelia of *Dolichos biflorus* agglutinin (DBA)–positive collecting ducts of Hoxb7-Plk4 P15 mice, in contrast with the normal centrosome number of control littermates (Fig. S6, B and C). Similarly, there was a slight but significant increase in the fraction of cells with CA in *Lotus tetragonolobus* lectin (LTL)–positive proximal tubules of Six2-Plk4 at P7 (Fig. S6, B and C). Next, we quantified ciliary abundance and length in cystic epithelia compared with normal nephron epithelia of control animals. There was a significant decrease in the fraction of cells that assembled a cilium in collecting ducts of Hoxb7-Plk4 P15 mice (Fig. 5, B and C), and in proximal tubules of Six2-Plk4 at P7 (Fig. 5, B and E). In addition, we noted a decrease in mean ciliary length in cystic cells that did assemble a cilium by P15, another important indicator of ciliary dysfunction (Fig. 5, D and F).

Cystogenesis is caused in part by inappropriate activation of several cellular signaling pathways (Bhaskar et al., 2015). One such pathway is the mammalian target of rapamycin (mTOR), which becomes hyperactive upon mutations in PKD genes (Shillingford et al., 2006; Boletta, 2009; Distefano et al., 2009; Dere et al., 2010) or after cilia ablation (Boehlke et al., 2010). Intriguingly, a link between CA and the mTOR protein complex was recently established, as mouse embryonic fibroblasts isolated from *tsc1*$^{-/-}$ and *tsc2*$^{-/-}$ mice were found to contain supernumerary centrosomes (Hartman et al., 2009). Moreover, we showed that *tsc1*$^{-/-}$ and *tsc2*$^{-/-}$ cells with excess centrosomes assembled excess cilia, displayed aberrant trafficking of ciliary proteins, and enhanced cell proliferation (Mahjoub and Stearns, 2012). Thus, we hypothesized that CA might be driving cystic epithelial proliferation in our animal models by causing inappropriate activation of mTOR signaling postnatally, when mTOR activity is naturally low. Indeed, immunoblot analysis of kidney lysates from P15 Hoxb7-Plk4 mice showed increased phosphorylation levels of S6 and S6-kinase (Fig. 5, G and H), downstream effectors of the mTOR complex and surrogate markers for pathway activation (Shillingford et al., 2006). Consistent with this observation, we noted a significant increase in proliferation of cyst-lining epithelial cells at P15, a stage when cell proliferation is low in control animals (Fig. 5, I and J). In sum, our results indicate that CA is sufficient to induce renal cystogenesis postnatally, likely via disruption of ciliary assembly/function and enhanced activity of the mTOR signaling pathway.

CA sensitizes mature kidneys to renal injury

Next, we sought to determine how centrosome perturbations affect the already differentiated, quiescent epithelia of mature nephrons in adult kidneys. There are at least two possible ways in which supernumerary centrosomes may perturb adult kidney homeostasis: (a) CA itself may be sufficient to trigger changes in quiescent epithelial cell physiology and cause cystogenesis, or (b) CA in adult kidneys may make them susceptible to cyst formation after renal injury, when early developmental signaling pathways initiate repair of damaged nephron epithelia. To distinguish between these possibilities, we induced mChPlk4 overexpression in distal tubule and collecting duct epithelia of mature nephrons by mating mChPlk4 with mice expressing Cre-recombinase under control of the cadherin-16 promoter (Shao et al., 2002; Fig. 1 A and Fig. S1 A; hereafter named Ksp-Plk4). Intriguingly, kidneys of P7-P30 Ksp-Plk4 mice were normal in size and morphology, with no cyst formation evident

fluorescence intensity was quantified by outlining each UB structure and the signal intensity measured and represented per unit area. For MM differentiation, the number of LEF1-positive cells per renal vesicle (adjacent to E-cadherin–positive UB structures) was scored. $n = 4$ for WT, Hoxb7-Plk4, and Six2-Plk4 mice. A two-tailed unpaired *t* test was used for statistical analysis (*, $P < 0.05$). **(E)** Representative images of E15.5 kidney sections from Six2-Plk4 and control mice stained for centrosomes (γ-tubulin), mitotic spindle microtubules (α-tubulin), mitotic marker (pHH3), and DNA (DAPI). In control kidneys, two centrosomes organize bipolar spindles that will eventually segregate the DNA into two daughter cells. When extra centrosomes are present, multipolar configurations are frequent (right). When centrosome clustering occurs (middle), the morphology of mitotic spindles appears bipolar (termed pseudobipolar). Bars (insets), 1 µm. **(F)** Quantification of the percentage of cells with bipolar and multipolar spindle configurations over time. In control animals that contain the normal complement of centrosomes, cells only form bipolar spindles in mitosis. To determine spindle morphologies in Hoxb7-Plk4 and Six2-Plk4 animals, quantification was done only in cells that contained excess centrosomes, as cells with normal centrosome number only form normal bipolar spindles (not depicted). In cells with CA, multipolar spindles are prevalent at early stages of development in both Hoxb7-Plk4 and Six2-Plk4 animals. However, cells with supernumerary centrosomes display pseudobipolar spindle morphologies at later development stages. $n = 5$ mice of each genotype from each developmental time point. A two-tailed unpaired *t* test was used to determine statistical significance (*, $P < 0.05$).

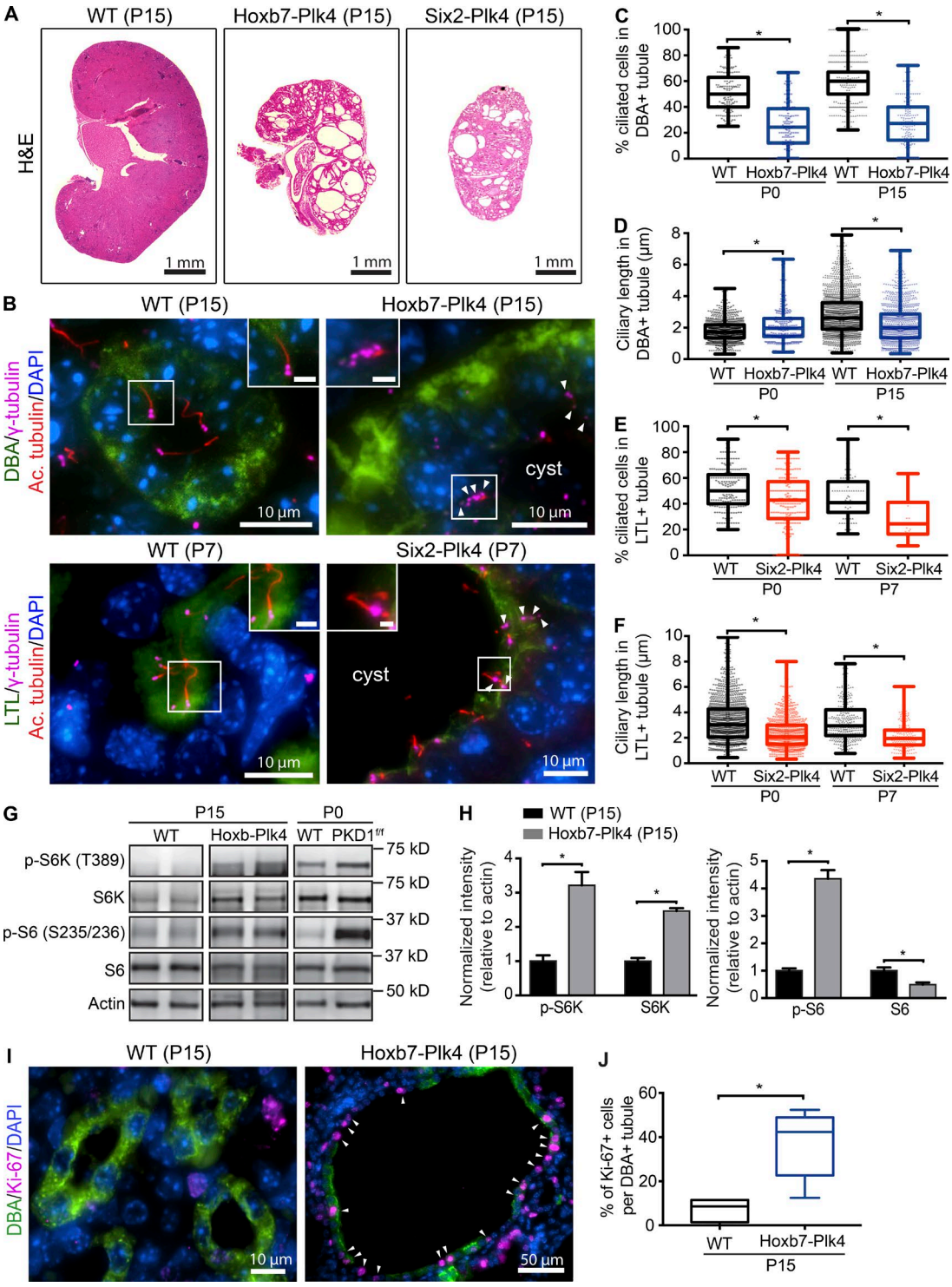

Figure 5. **CA causes cystogenesis. (A)** H&E-stained kidney sections from postnatal (P15) Hoxb7-Plk4, Six2-Plk4, and control mice. **(B)** Immunostaining of P15 and P7 sections for centrosomes (γ-tubulin), cilia (acetylated α-tubulin), proximal tubules (LTL), collecting ducts (DBA), and nuclei (DAPI). Cells from control animals contained the normal complement of centrosomes and assembled a single cilium. In contrast, CA disrupted ciliogenesis, resulting in aciliated cells or formation of short cilia. White box denotes regions shown in insets. Arrowheads point to cells with multiple centrosomes. Bars (insets), 2 µm. **(C)** Graph illustrating a decrease in the fraction of ciliated cells in collecting ducts of P0 to P15 Hoxb7-Plk4 kidneys. *n* = 1,971 cells from 186 tubules (P0 WT), 1,769 cells from 135 tubules (P0 Hoxb7-Plk4), 2,550 cells from 411 tubules (P15 WT), and 3,541 cells from 149 cysts (P15 Hoxb7-Plk4). **(D)** Quantification of the length of cilia in cystic epithelia of Hoxb7-Plk4 kidneys, demonstrating a small but significant decrease in mean ciliary length by P15. *n* = 951 cilia measured (P0 WT), 314 cilia (P0 Hoxb7-Plk4), 1,852 cilia (P15 WT), and 1,186 cilia (P15 Hoxb7-Plk4). **(E)** Graph demonstrating a decrease in the fraction of ciliated cells in proximal tubules of P0 to P7 Six2-Plk4 kidneys. *n* = 2,218 cells from 251 tubules (P0 WT), 1,637 cells from 188 tubules (P0 Six2-Plk4), 643 cells from 91 tubules (P7 WT), and 678 cells from 24 cysts (P7 Six2-Plk4). **(F)** Graph illustrating decreased ciliary length in cystic epithelia of Six2-Plk4 kidneys by P7. *n* = 1,363 cilia measured (P0 WT), 811 cilia (P0 Six2-Plk4), 329 cilia (P7 WT), and 216 cilia (P7 Six2-Plk4). For all graphs, a two-tailed unpaired *t* test was performed to determine statistically significant differences (*, P < 0.05). **(G and H)** Representative immunoblots of kidney lysates demonstrating that phosphorylated ribosomal protein S6 (p-S6)

(Fig. 6 A). Furthermore, we did not observe any cysts in Ksp-Plk4 kidneys up to 1 yr of age (not depicted). Immunostaining of P30 Ksp-Plk4 kidneys showed robust expression of mChPlk4 in distal tubules (chloride channel-K [CLC-K]–positive) and collecting ducts (DBA-positive) as expected; thus, the lack of cystic phenotype was not a result of absence of Plk4 overexpression (Fig. 6 B). We quantified the number of centrosomes in collecting duct epithelia of Ksp-Plk4 animals at P30 and found that Plk4 overexpression indeed resulted in CA in these cells (Fig. 6, C and D). Moreover, cells with CA displayed ciliary assembly defects consistent with our two embryonic models (Fig. 6, C–E). Thus, CA in mature nephrons can disrupt ciliary homeostasis without inducing cystogenesis, highlighting intrinsic differences between the active state of proliferation during development versus quiescent differentiated cells.

Although the ablation of cilia during gestation results in severe cystic disease shortly after birth, loss of cilia in the adult kidney does not cause rapid cystogenesis (Davenport et al., 2007). Eventually, mild cyst formation occurs 6–12 mo after loss of cilia, revealing different requirements of ciliary function during renal development versus maintenance in adult kidneys (Davenport et al., 2007). However, the cystic phenotype is accelerated by the induction of ischemia-reperfusion injury (IRI) or pharmacological nephrotoxicity, models that induce renal regeneration (Kobayashi et al., 2008; Patel et al., 2008; Takakura et al., 2009). Thus, we tested whether kidneys of adult Ksp-Plk4 were susceptible to renal injury. We performed unilateral IRI on 3-mo-old Ksp-Plk4 mice and their littermate controls by clamping the left renal pedicle (Patel et al., 2008; Takakura et al., 2009). Remarkably, the injured kidneys rapidly developed cysts that were evident 30 d after IRI, whereas the contralateral (nonischemic) kidneys were unaffected (Fig. 6 F). Collectively, our results suggest that CA sensitizes mature kidneys, such that they become rapidly cystic after renal insult.

CA and ciliogenesis defects in human polycystic kidney disease (PKD)

To examine the extent of CA and its effects on ciliary assembly in cystic disease models in vivo, we analyzed kidneys from patients with ADPKD, as it is the most common form of cystic kidney disease and samples are readily available (compared with other much rarer hereditary cystic nephropathies). Centrosomes were marked with antibodies against γ-tubulin or centrin, two core components of the centrosome (Nigg and Stearns, 2011; Brito et al., 2012; Goto et al., 2013), and bona fide centrosomes quantified using γ-tubulin. We found that CA is highly prevalent in cystic epithelial cells, but extremely rare in healthy kidney cells (Fig. 7, A and B). Cystic cells in PKD samples displayed a wide range in the levels of CA, from mild to severe (Fig. 7 B). Because cysts develop spontaneously over the lifespan of affected individuals, there are various "generations" of cysts, with cells that have experienced transformative events for different lengths of time or rates of expansion. By comparing small and large cysts, we noted that CA is evident early during cyst formation and persists as the cysts increase in size (Fig. 7 E). Importantly, a significant number of cells possessing excess centrosomes were either aciliated or superciliated (Fig. 7, C, D, and F), which corresponded with a decrease in the percentage of cells containing a single cilium, highlighting a detrimental effect on ciliogenesis. Collectively, these data indicate that the defects in ciliary assembly upon CA that we observed in vitro (Mahjoub and Stearns, 2012) and in our mouse models in vivo (Figs. 4 and 5) are recapitulated in ADPKD tissues in vivo.

Discussion

Here, we performed a comprehensive analysis of the consequences of CA during embryonic kidney development, at adult kidney homeostasis, and after renal injury. We discovered that CA in renal progenitor cells causes decreased progenitor cell proliferation and differentiation, increased apoptosis, and consequently, hypoplastic kidneys. These are reminiscent of cellular defects observed in the developing brain, where CA was shown to cause loss of the progenitor population because of increased apoptosis, resulting in small brains (microcephaly; Marthiens et al., 2013). Importantly, we show that CA is sufficient to induce cystogenesis shortly after birth. The cystic phenotype is likely caused by a combination of (a) defects in nephron formation seen during embryogenesis that can result in nephron obstruction, and (b) ciliogenesis defects that persist when renal development is completed. The cystic phenotype appeared independently of mutations in cystic genes, suggesting that CA is in itself detrimental to renal growth and homeostasis.

To our best knowledge, this is the first demonstration that CA is sufficient in causing a ciliopathy phenotype in vivo. This discovery is in stark contrast with studies focusing on the relationship between CA and tumorigenesis, where widespread or tissue-specific induction of CA did not lead to spontaneous tumor formation (Marthiens et al., 2013; Coelho et al., 2015; Kulukian et al., 2015; Vitre et al., 2015; Serçin et al., 2016). A recent study did note that global induction of CA could initiate spontaneous formation of lymphomas and squamous cell carcinomas in aged mice (Levine et al., 2017), highlighting the heterogeneity of the response to CA in different tissues and developmental stages. Indeed, we found that CA in differentiated epithelia of matured nephrons did not affect the quiescent state of the cells, nor cause their untimely proliferation. This is consistent with the observation that loss of cilia in quiescent cells of fully formed

and p-S6K increase upon CA. Two examples are shown for control (WT) and Hoxb7-Plk4. Kidney lysates obtained from Hoxb7-*PKD1*$^{f/f}$ mice were used as a positive control for pathway activation. Total levels of S6 were mostly unchanged, whereas total S6K was also elevated. Graph shows quantifications of band signal intensity, normalized to actin for each marker. n = 3 kidneys from each genetic sample; (*, P < 0.05). **(I)** Representative images of P15 kidney sections from control and Hoxb7-Plk4 mice, immunostained with antibodies against Ki-67, DBA, and DAPI. Proliferating Ki-67–positive cells are highlighted with white arrowheads. **(J)** Graph denoting the percentage of Ki-67–positive cells in DBA-positive collecting ducts (WT) or cysts (Hoxb7-Plk4). A two-tailed unpaired t test was used to determine statistically significance (*, P < 0.05).

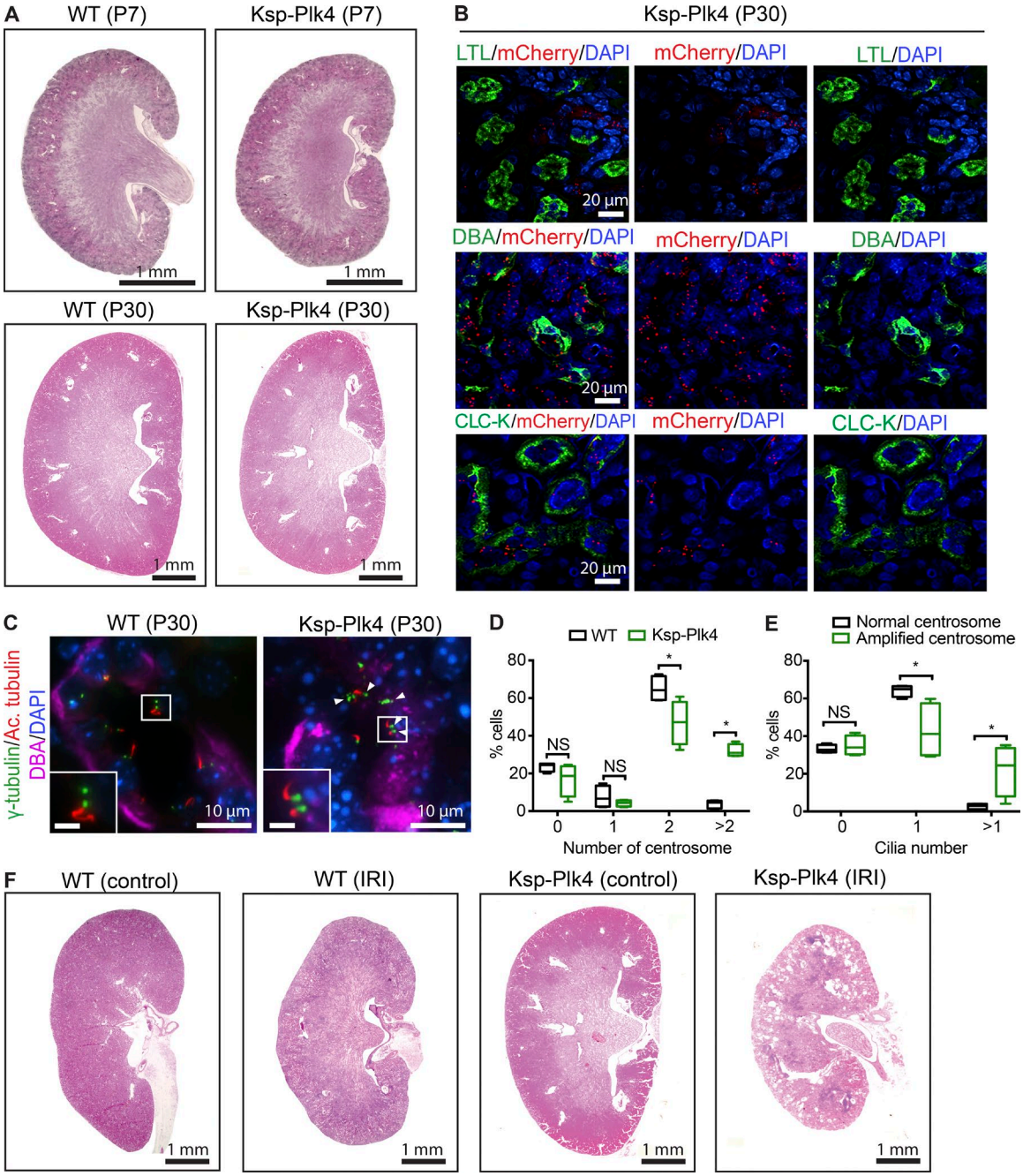

Figure 6. **CA in adult mice sensitizes kidneys to renal injury. (A)** H&E staining of control and Ksp-Plk4 kidneys isolated at P7 and P30. No prominent cysts were evident at these stages. **(B)** Kidney samples from P30 Ksp-Plk4 mice immunostained with anti-mCherry to identify cells expressing mChPlk4. There was robust expression of Plk4 in DBA-positive collecting ducts and CLC-K–positive distal tubules, but absent in LTL-positive proximal tubules, consistent with Ksp-Cre–mediated expression. Nuclei were stained with DAPI. **(C)** Immunostaining of P30 control and Ksp-Plk4 kidneys to mark centrosomes (γ-tubulin), cilia (acetylated α-tubulin), collecting ducts (DBA), and DNA (DAPI). In contrast to the normal centrosome number in control kidneys, CA is evident in Ksp-Plk4. White box denotes regions shown in insets. Arrowheads point to cells with multiple centrosomes and cilia. Bars (insets), 2 µm. **(D)** Quantification of CA in P30 WT and Ksp-Plk4 mice. *n* = 747 cells (WT) and 562 cells (Ksp-Plk4). **(E)** Quantification of the percentage of cells expressing zero, one, or more than one primary cilium in P30 Ksp-Plk4 mice containing excess centrosomes compared with cells with normal centrosome number. CA caused an increase in the fraction of superciliated cells. *n* = 274 cells (WT) and 172 cells (Ksp-Plk4). Statistical significance was determined using a two-tailed unpaired *t* test (*, $P < 0.05$). **(F)** H&E staining of kidneys after unilateral renal IRI. Ischemic injury was induced in 3-mo-old Ksp-Plk4 mice and littermate controls by clamping the left renal pedicle for 45 min. Kidneys were isolated 30 d after IRI. Injured kidneys of Ksp-Plk4 mice rapidly developed cysts, which were absent in the contralateral (uninjured) kidney, as well as the injured kidney of control mice. *n* = two mice (WT control) and five mice (Ksp-Plk4).

adult kidneys does not disrupt renal morphology or function (Davenport et al., 2007). The detrimental effects of CA were felt after renal insult, when cellular proliferation is triggered to help repair damaged nephron epithelia (Chang-Panesso and Humphreys, 2017), a process that is cilia-dependent (Kobayashi et al., 2008; Patel et al., 2008; Takakura et al., 2009).

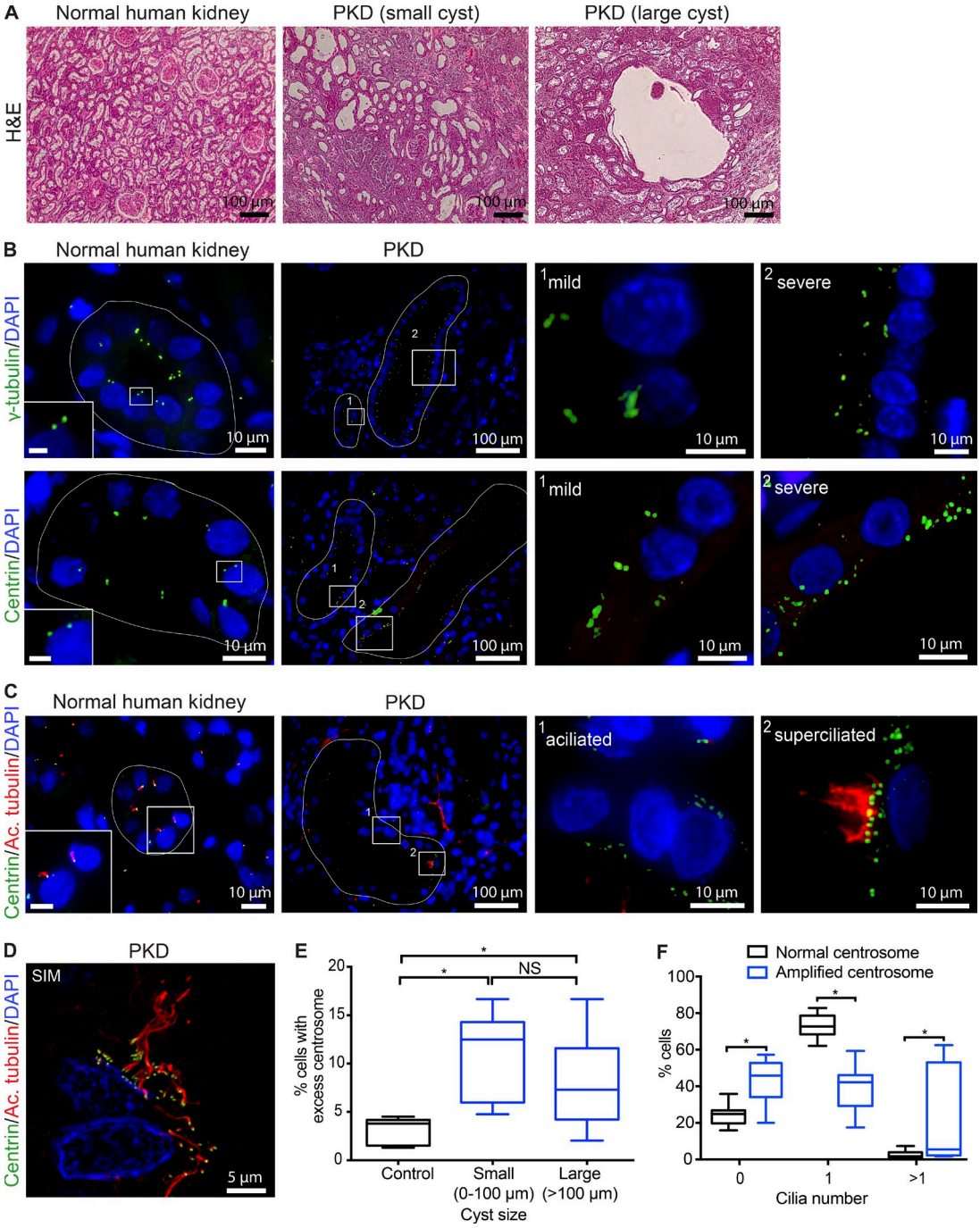

Figure 7. **Cystic epithelia in human PKD display CA and ciliogenesis defects. (A)** H&E staining of normal and ADPKD kidney sections showing the typical architecture of renal tubules, compared with small and large cysts in PKD samples, respectively. **(B)** Immunofluorescence staining of normal and PKD kidney specimens with antibodies against γ-tubulin or centrin to identify centrosomes, and DAPI to mark nuclei. Normal kidney epithelia predominantly contained the normal complement of centrosomes (one to two foci), whereas a significant fraction of cystic epithelia contained greater than two foci per cell. Cystic tubules of PKD patients display both low (mild) and high (severe) levels of CA. White lines in normal kidneys outline a typical nephron tubule, and cysts of different sizes in PKD samples. Bars (insets), 2 µm. **(C)** Normal and PKD kidney sections were immunostained for centrosomes and cilia. Normal kidney cells contain one centrosome and assemble a single primary cilium (inset magnified twofold). Cystic cells containing excess centrosomes either fail to assembly a cilium (aciliated) or form more than one cilium (superciliated). Nuclei were stained with DAPI. Bars (insets), 5 µm. **(D)** Representative image of cystic cells in PKD tissue captured using superresolution SIM, highlighting the presence of more than one cilium in cells with CA. **(E)** Quantification of the percentage of cells with CA relative to cyst size. Centrosomes were marked with γ-tubulin, and centrosome number quantified per nucleus in normal nephron epithelia (control) and epithelial cells lining the cyst walls (PKD). n = 961 cells from 80 tubules analyzed from four normal kidneys, 501 cells from 40 small cysts (0–100 µm), and 1,423 cells from 37 large cysts (>100 µm) in seven PKD patient samples. Box plots represent the median, maximum, and minimum values for each dataset. One-way ANOVA was performed to determine statistically significant differences between samples (*, $P < 0.05$). **(F)** Quantification of ciliary defects in cystic epithelia of PKD patients. The percentage of cells with zero, one, or more than one cilium was determined from cyst-lining cells that contained either normal centrosome number, compared with cells with CA. n = 1,521 cells scored from eight PKD kidneys. Statistical significance was calculated using a two-tailed unpaired t test (*, $P < 0.05$).

In dividing cells, CA can cause spindle assembly defects, chromosome missegregation, and aneuploidy, triggering a p53-mediated surveillance mechanism that clears cells with abnormal chromosome number (Nano and Basto, 2016). We found that multipolar spindles were only detected during early developmental stages, which coincided with increased apoptosis and reduced proliferation. Thus, we posit that the observed apoptosis of the renal progenitor population may be at least partially a result of the p53-mediated surveillance mechanism. One way to test this would be to delete one or both copies of p53, which can enhance survival of cells with CA and help promote tumor growth (Coelho et al., 2015; Serçin et al., 2016). However, conditional inactivation of p53 in embryonic kidneys delays UB branching, disrupts proliferation of MM, and causes renal hypoplasia (Saifudeen et al., 2009, 2012). Thus, we could not test the synergistic effects of CA and p53 directly in the kidney. However, we found that cells predominantly formed pseudobipolar spindles after E15.5 even when they had extra centrosomes. This suggests that renal progenitors either lack the capacity to cluster their centrosomes at early developmental stages, or acquire the mechanisms that promote clustering at later stages, which helps in the survival of cells that proliferate and subsequently form cysts.

In addition to the mitotic defects, CA has a detrimental effect on ciliary assembly and function. In a landmark study, we showed that CA in cultured cells either blocked assembly, or resulted in the formation of excess cilia (Mahjoub and Stearns, 2012). The net phenotypic outcome was the same, in that disrupted signaling in the former was a result of loss of the chemo/mechanosensory apparatus itself, whereas the latter was a result of inefficient operation of the signaling machinery. We found that CA in kidneys of PKD patients and our mouse models caused similar ciliogenesis defects. Moreover, cystic livers of *PKD2* mice also contain excess centrosomes and ciliary assembly defects (Masyuk et al., 2014), indicating that ciliary function is likely abrogated upon CA in other cell types. How do CA and the associated ciliary defects perturb embryonic renal development and subsequently drive cystogenesis? Genetic ablation of cilia in embryonic kidneys disrupts signaling pathways essential for progenitor cell expansion (Chi et al., 2013), including the WNT11/RET-ERK pathway needed for UB branching morphogenesis, and the WNT4-LEF1 pathway necessary to maintain the MM population (Fisher et al., 2001; Majumdar et al., 2003; Schmidt-Ott and Barasch, 2008; Mugford et al., 2009; Brown et al., 2013). Analysis of these signaling pathways showed that they are attenuated in our mice, suggesting that CA in embryonic kidneys compromises these essential developmental signaling cascades. In adult kidneys, CA may similarly disrupt cilia-dependent signaling pathways that contribute to cystogenesis. Indeed, we found that the mTOR signaling pathway activity was elevated/sustained in our cystic animal models postnatally. Thus, one enticing possibility is that CA may be a common cellular aberration linking mutations in various cystic genes, ciliary signaling dysfunction, and activation of signaling pathways that promote cell proliferation. Our future studies will focus on defining the synergistic effects of CA in the context of mutations in different cyst-inducing genes, and test whether CA offers a potentially new therapeutic target for the treatment of cystic diseases of the kidney.

Materials and methods

Transgenic animals

All animal studies were performed following protocols that are compliant with guidelines of the Institutional Animal Care and Use Committee at Washington University and the National Institutes of Health. Transgenic mCherry-Plk4 animals were originally generated in C57BL6/N background (Marthiens et al., 2013) and were maintained in a heterozygous state (Tg[mChPlk4]/+) by mating with C57BL6/N WT mice. To induce expression of mChPlk4 in the UB, heterozygous Tg(mChPlk4)/+ animals were bred with mice that express the UB-specific Cre-recombinase under the control of the Hoxb7 promoter (Zhao et al., 2004; Hoxb7-Cre^{GFP}/+). This mating scheme resulted in experimental animals that were heterozygous for each transgene (Tg[mChPlk4]/+; Hoxb7-Cre^{GFP}/+), and littermates carrying the single transgenes alone (Tg[mChPlk4]/+ or Hoxb7-Cre^{GFP}/+) were used as our WT control. To induce expression of mChPlk4 in the MM, heterozygous Tg(mChPlk4)/+ animals were bred with mice that express mesenchyme-specific Cre-recombinase under the control of the Six2 promoter (Kobayashi et al., 2008; Six2-Cre^{GFP}/+). This mating scheme resulted in experimental animals that were heterozygous for each transgene (Tg[mChPlk4]/+; Six2-Cre^{GFP}/+), and littermates carrying the single transgenes alone (Tg[mChPlk4]/+ or Six2-Cre^{GFP}/+) were used as control. Finally, we induced expression of mChPlk4 in the distal tubule and collecting duct epithelia of mature nephrons by crossing Tg(mChPlk4)/+ animals with heterozygous mice expressing Cre-recombinase under the control of the cadherin-16 promoter (Shao et al., 2002; Ksp-Cre/+). This mating scheme resulted in experimental animals that were heterozygous for each transgene (Tg[mChPlk4]/+; Ksp-Cre/+), and littermates carrying the single transgenes alone (Tg[mChPlk4]/+ or Ksp-Cre/+) were used as control.

For timed pregnancies, the day of the copulatory plug was defined as E0.5. Crosses were equally performed with males and females of each transgenic strain, and embryos, pups, and adults from both genders were included in the analyses. Genotyping was performed by extracting tail DNA followed by PCR using the following primers: mChPlk4 (706 bp): 5′-CGCCACCATGGTGAG GAAGGG-3′ and 5′-CTCGTCCATGCCGCCGGTGG-3′; Hoxb7-Cre^{GFP} (237 bp): 5′-GCAGAACCTGAAGATGTTCGCGAT-3′ and 5′-ATGAGT GAACGAACCTGGTCGAAA-3′; Six2-Cre^{GFP} (420 bp): 5′-TCGATG CAACGAGTGATGAG-3′ and 5′-TCCATGAGTGAACGAACCTG-3′; and Ksp-Cre (390 bp): 5′-GCAGATCTGGCTCTCCAACG-3′ and 5′-AGGCAAATTTTGGTGTACGG-3′. Kidneys were isolated from experimental and control animals at various stages of embryonic development (E12.5, E13.5, E15.5, and E17.5) and postnatally (P0, P7, P15, and P30). A summary of the number of animals isolated and analyzed from each genotype is provided in Table S1.

Immunological analysis of kidneys

Both kidneys were isolated from each embryo or adult mouse as previously described (Hoshi et al., 2015) and fixed in one of two ways, depending on the downstream application. Specimens were fixed in 4% paraformaldehyde in PBS for 24 h at 4°C, then embedded in paraffin. Samples were cut into 5-µm sections using a microtome (RM2125 RTS; Leica), placed onto microscope slides (Thermo Fisher Scientific), and stored at room temperature.

Alternatively, freshly isolated kidneys were placed in appropriately sized Cryomolds (Tissue-Tek), immersed in Optimal Cutting Temperature compound (Tissue-Tek), and placed in a dry ice/ethanol bath for 10 min. Frozen samples were cut into 10-µm sections using a cryostat (CM1850; Leica), placed onto microscope slides, and stored at −80°C. Histological staining of paraffin-embedded sections with hematoxylin and eosin (H&E) was performed using standard protocols (Hoshi et al., 2015).

For immunohistochemistry on paraffin-embedded sections, antigen unmasking was performed by boiling the slides in antigen-retrieval buffer (10 mM Tris Base, 1 mM EDTA, and 0.05% Tween-20, pH 9.0) for 30 min. For immunostaining of cryopreserved sections, samples were fixed using −20°C-precooled methanol for 10 min. After fixation, both types of fixed samples were preextracted with 0.5% Triton X-100 in PBS for 10 min at room temperature and incubated in blocking buffer (3.0% BSA and 0.5% Triton X-100 in PBS) for 1 h, followed by staining with primary and secondary antibodies. The complete list of antibodies and nephron segment markers used in this study is provided in Table S2. All Alexa Fluor dye–conjugated secondary antibodies were obtained from Thermo Fisher Scientific and used at a final dilution of 1:500. Nuclei were stained with DAPI, and specimens mounted using Mowiol containing *n*-propyl gallate (Sigma-Aldrich). Images were captured using a Nikon Eclipse Ti-E inverted confocal microscope equipped with 10× Plan Fluor (0.30 NA), 20× Plan Apo air (0.75 NA), 60× Plan Fluor oil immersion (1.4 NA), or 100× Plan Fluor oil immersion (1.45 NA) objectives (Nikon). A series of digital optical sections (z-stacks) were captured using an Andor Neo-Zyla CMOS camera at room temperature, and three-dimensional image reconstructions were produced. Images were processed and analyzed using Elements AR 4.20 (Nikon) and Photoshop software (Adobe).

Evaluation of the number of centrosomes and cilia

For quantification of centrosome and cilia number in renal progenitors and differentiated nephron epithelia, a minimum of five tissue sections—a midsagittal section and sections generated in 20-µm increments in both directions from the midsagittal section—were analyzed. Samples were stained with antibodies against mCherry to identify cells expressing mChPlk4. Centrosomes were identified by costaining cells with antibodies targeting γ-tubulin and centrin. We considered foci as centrosomes only if they stained with at least two of the centrosome markers. Normal centrosome number was defined as cells containing one or two foci of γ-tubulin, and CA was characterized by the presence of more than two foci per cell. Centrosome number was quantified per nucleus of the cells in each cell population, using cell-specific markers to outline individual cells (e.g., using E-cadherin or Six2). Cilia were identified as acetylated tubulin-positive structures emanating from γ-tubulin/centrin-positive centrosomes. Primary cilium assembly was determined by counting the percentage of cells that formed zero, one, or more than one cilium per cell. Ciliary length was measured from three-dimensional reconstructions of z-stack images, using integrated image analysis software (Nikon Elements AR 4.20). For all of the above analyses, sections were costained with antibodies to help identify mesenchymal progenitor cells (Six2-positive), glomerular precursor cells (WT1-positive), and UB structures (E-cadherin– or CK8-positive) in embryonic kidneys. For postnatal kidneys, samples were costained with nephron segment markers including LTL (marker of proximal tubules; Vector Laboratories), antibodies against the chloride channel CLC-K (marker of distal tubules; Alomone Labs; gift of F. Chen, Washington University, St. Louis, MO), and DBA (marker of collecting ducts; Vector Laboratories).

For evaluation of mitotic spindle morphology, paraffin-embedded embryonic and postnatal kidney specimens were immunostained for γ-tubulin (centrosomes), α-tubulin (microtubules), pHH3 (mitotic marker), and DNA (DAPI). Three-dimensional reconstructions of z-stack images were used for the analysis. To determine the fraction of cells with abnormal spindle morphology, we counted all prometaphase or metaphase cells in each kidney section containing more than one centrosome, and compared that with mitotic cells containing the normal complement of two centrosomes.

Analysis of renal progenitor cell proliferation, differentiation, and apoptosis

The mean number of mesenchymal cells per MM cap structure was determined by counting the number of Six2-positive cells per UB branch tip. At least 25 cap structures/UB tips were scored per genotype for each indicated time point. To estimate the differentiation potential of the MM progenitor cells, the mean number of WT1-positive structures was counted per section. A minimum of five kidney section—a midsagittal section and sections generated 20 µm in both directions—was analyzed from E15.5 and E17.5 embryos. Proliferation analysis was performed by measuring the number of pHH3-positive mitotic cells per section. Because the size of kidneys from Tg(mChPlk4)/+; Hoxb7-Cre^{GFP}/+ and Tg(mChPlk4)/+; Six2-Cre^{GFP}/+ are smaller than the control kidneys, the area of each section was also measured. The data are expressed as the mean number of pHH3-positive foci per unit area (squared millimeter) of each kidney section. The TUNEL method was used to quantify apoptosis, following the manufacturer's instructions (In Situ Cell Death Detection kit; Roche). Kidneys specimens from E15.5 and E17.5 animals were processed for immunofluorescence (Jain et al., 2006) as described above, and the mean number of TUNEL-positive cells per unit area (squared millimeter) of each kidney was determined. Nephron endowment at birth was determined using two complementary approaches: (a) by staining P0 kidney sections with antibodies against Podocin (gift of J. Miner, Washington University, St. Louis, MO), a marker of glomeruli (Roselli et al., 2002), and (b) by counting the number of glomeruli directly in H&E-stained tissue sections. The mean number of glomeruli per section was then calculated from a minimum of five sections from experimental and control animals of each genotype.

Live-cell imaging of embryonic kidneys

Isolation, growth, and imaging of metanephric organ cultures were performed as previously described (Keefe Davis et al., 2013; Hoshi et al., 2015). In brief, kidneys were isolated from Hoxb7-Cre^{GFP} and Hoxb7-Cre^{GFP}-Plk4 embryos at E12.5, and from Six2-Cre^{GFP} and Six2-Cre^{GFP}-Plk4 embryos at E13.5. Kidneys were cultured on 0.4-µm pore Transwell membranes (Corning) in

a six-well culture plate for up to 72 h. Samples were grown in DMEM/F12 containing 15 mM Hepes, supplemented with 0.01 nM prostaglandin E1, 5 mg/ml ion-saturated holo Transferrin, and 10 nM sodium selenite (all from Sigma-Aldrich). Culture medium was changed every 24 h. Time-lapse microscopy was performed in a temperature-controlled culture chamber with a 5% CO_2 air mixture. Images were captured at 30-min intervals for up to 48 h. For quantification of ureteric bud tips, E12.5 metanephric kidneys were cultured and all tips counted in a blinded fashion from images captured at the indicated times. Kidneys with three to five UB tips at the beginning of organ culture were used for this analysis.

Immunoblot analysis of kidney lysates

Kidneys were collected and homogenized in T-PER lysis buffer (Thermo Fisher Scientific) supplemented with protease (Pierce) and phosphatase inhibitors (Roche). The homogenized lysate was incubated at 4°C for 20 min and cell debris cleared by centrifugation at 12,000 *g* for 10 min. 50 µg of protein lysate from each kidney was analyzed by SDS-PAGE. Membranes were incubated overnight at 4°C with the following primary antibodies: anti–phospho-p-S6K (1:200; Tyr 389; 9205; Cell Signaling Technology), anti-p-S6K (1:1,000; sc-8418; Santa Cruz Biotechnology), anti–phospho-S6 (1:200; Ser235/236; 2211; Cell Signaling Technology), anti-S6 (1:500; sc-74459; Santa Cruz Biotechnology), and anti-actin (1:1,000; A4700; Sigma-Aldrich). Secondary antibodies included donkey anti–rabbit IgG–horseradish peroxidase (Sigma-Aldrich) and goat anti–mouse IgG–horseradish peroxidase (Jackson ImmunoResearch Laboratories). Blots were imaged on a C-DiGit Blot Scanner (LI-COR), and signal intensities for each protein were quantified and normalized to actin.

IRI

Unilateral IRI was performed on Ksp-Plk4 and control (Ksp-Cre) littermates as previously described (Takakura et al., 2009). In brief, 3-mo-old animals were anesthetized with a mixture of ketamine (100 mg/kg body weight) and xylazine (15 mg/kg body weight) intraperitoneally before surgery. Body temperatures were controlled at 36.5–37.5°C throughout the procedure using a heating pad (Harvard Apparatus) and monitored using a rectal probe. Kidneys were exposed through flank incisions, and mice subjected to ischemia by clamping the left renal pedicle with nontraumatic vascular clamps (Fine Science Tools), which were removed after 45 min. Mice were sacrificed 30 d after surgery, and both the injured and contralateral (uninjured) kidneys from each animal isolated and analyzed as described above.

Analysis of human PKD specimens

Human kidney samples were obtained from archived materials stored in the Kidney Translational Research Center (Washington University in St. Louis) according to the guidelines of a protocol approved by the Institutional Review Board of the Washington University School of Medicine. Renal specimens were fixed in formalin and embedded in paraffin, and 5-µm sections were cut and placed onto microscope slides. Sections from eight ADP KD patients, with ages ranging from 56–75 yr, were used for analysis. Four kidney specimens with no cystic pathology from nontumorigenic regions of patients (age range of 48–61 yr) undergoing nephrectomy were used as controls. Specimens were processed and stained with antibodies to mark centrosomes and cilia as described above. Centrosome number and ciliogenesis were quantified in cystic epithelia of small (less than 100 µm diameter) and larger (>100 µm diameter) cysts in each kidney. In control specimens, epithelial cells of both tubular and collecting duct segments of the nephron were counted. Superresolution structured illumination microscopy (SIM) was performed on an n-SIM inverted Ti-E microscope (Nikon), which enabled simultaneous two-color and sequential four-color superresolution imaging. Images were captured and analyzed using Elements AR 4.20 (Nikon) software.

Statistical analysis

Statistical analyses were performed using GraphPad PRISM 7.0 or Microsoft Excel. The vertical segments in box plots show the first quartile, median, and third quartile. The whiskers on both ends represent the maximum and minimum values for each dataset analyzed. Collected data were examined by one-way ANOVA or two-tail unpaired *t* test as specified in the figure legends. Data distribution was assumed to be normal, but this was not formally tested. Statistical significance was set at $P < 0.05$.

Online supplemental material

Fig. S1 shows mouse models used for inducing CA in renal cells. Fig. S2 shows conditional Plk4 expression in the developing mouse kidney at E13.5. Fig. S3 shows conditional Plk4 expression in the developing mouse kidney at E15.5. Fig. S4 shows conditional Plk4 expression in the developing mouse kidney at E17.5. Fig. S5 shows that Plk4 overexpression causes CA and ciliogenesis defects in renal progenitors. Fig. S6 shows that CA causes cystogenesis. Table S1 is a summary of the total number of mice generated and analyzed by mating. Table S2 is a detailed list of antibodies and other reagents used in this study. Video 1 shows live-cell imaging of ex vivo metanephric organ cultures from Six2-CreGFP and Six2-CreGFP-Plk4 embryos. Video 2 shows live-cell imaging of ex vivo metanephric organ cultures from Hoxb7-Cre^{GFP} and Hoxb7-Cre^{GFP}-Plk4 embryos.

Acknowledgments

We thank R. Nanjundappa and X. Jin for their help with some experiments. We also thank J. Miner, F. Chen, and the Kidney Translational Research Center (Washington University, St. Louis, MO; DK079333) for sharing reagents used in this study. We thank Diane Salamon (Kidney Translational Research Center) for help in procuring patient specimens.

This project was supported by funding from a National Institutes of Health postdoctoral training grant (T32DK007126) to L.K. Dionne, Worldwide Cancer Research (13-0170) to V. Marthiens and R. Basto, and the National Institute of Diabetes and Digestive and Kidney Diseases (R01-DK082531) to S. Jain and (R01-DK108005) to M.R. Mahjoub.

The authors declare no competing financial interests.

Author contributions: L.K. Dionne performed the majority of the experimental work and data quantitation, prepared the

figures, and helped write the manuscript. K. Shim performed the mouse genetic crosses, isolated the kidneys, and prepared them for analysis. M. Hoshi performed the IRI and live-cell imaging experiments. T. Cheng helped in the quantitation of cell proliferation, apoptosis, developmental signaling pathways, and spindle assembly defects. J. Wang contributed to the generation of the Ksp-Cre-Plk4 mice. V. Marthiens and R. Basto developed and shared the transgenic Plk4 mouse model. A. Knoten provided technical assistance with mouse husbandry. S. Jain provided technical expertise in renal biology, shared reagents and mouse strains, and helped analyze the data. M.R. Mahjoub conceived the project, wrote the manuscript, and supervised all aspects of the project. All authors read and edited the manuscript.

Submitted: 4 October 2017
Revised: 23 October 2017
Accepted: 9 May 2018

References

Arquint, C., A.M. Gabryjonczyk, and E.A. Nigg. 2014. Centrosomes as signalling centres. *Philos. Trans. R. Soc. Lond. B Biol. Sci.* 369:20130464. https://doi.org/10.1098/rstb.2013.0464

Astrinidis, A., W. Senapedis, and E.P. Henske. 2006. Hamartin, the tuberous sclerosis complex 1 gene product, interacts with polo-like kinase 1 in a phosphorylation-dependent manner. *Hum. Mol. Genet.* 15:287–297. https://doi.org/10.1093/hmg/ddi444

Battini, L., S. Macip, E. Fedorova, S. Dikman, S. Somlo, C. Montagna, and G.L. Gusella. 2008. Loss of polycystin-1 causes centrosome amplification and genomic instability. *Hum. Mol. Genet.* 17:2819–2833. https://doi.org/10.1093/hmg/ddn180

Bettencourt-Dias, M., F. Hildebrandt, D. Pellman, G. Woods, and S.A. Godinho. 2011. Centrosomes and cilia in human disease. *Trends Genet.* 27:307–315. https://doi.org/10.1016/j.tig.2011.05.004

Bhaskar, L.V., R. Elumalai, and S. Periasamy. 2015. Pathways, perspectives and pursuits in polycystic kidney disease. *J. Nephropharmacol.* 5:41–48.

Boehlke, C., F. Kotsis, V. Patel, S. Braeg, H. Voelker, S. Bredt, T. Beyer, H. Janusch, C. Hamann, M. Gödel, et al. 2010. Primary cilia regulate mTORC1 activity and cell size through Lkb1. *Nat. Cell Biol.* 12:1115–1122. https://doi.org/10.1038/ncb2117

Boletta, A. 2009. Emerging evidence of a link between the polycystins and the mTOR pathways. *PathoGenetics.* 2:6. https://doi.org/10.1186/1755-8417-2-6

Brito, D.A., S.M. Gouveia, and M. Bettencourt-Dias. 2012. Deconstructing the centriole: structure and number control. *Curr. Opin. Cell Biol.* 24:4–13. https://doi.org/10.1016/j.ceb.2012.01.003

Brown, A.C., S.D. Muthukrishnan, J.A. Guay, D.C. Adams, D.A. Schafer, J.L. Fetting, and L. Oxburgh. 2013. Role for compartmentalization in nephron progenitor differentiation. *Proc. Natl. Acad. Sci. USA.* 110:4640–4645. https://doi.org/10.1073/pnas.1213971110

Burtey, S., M. Riera, E. Ribe, P. Pennenkamp, R. Rance, J. Luciani, B. Dworniczak, M.G. Mattei, and M. Fontés. 2008. Centrosome overduplication and mitotic instability in PKD2 transgenic lines. *Cell Biol. Int.* 32:1193–1198. https://doi.org/10.1016/j.cellbi.2008.07.021

Chang-Panesso, M., and B.D. Humphreys. 2017. Cellular plasticity in kidney injury and repair. *Nat. Rev. Nephrol.* 13:39–46. https://doi.org/10.1038/nrneph.2016.169

Chen, Y., H.C. Chiang, P. Litchfield, M. Pena, C. Juang, and D.J. Riley. 2014. Expression of Nek1 during kidney development and cyst formation in multiple nephron segments in the Nek1-deficient kat2J mouse model of polycystic kidney disease. *J. Biomed. Sci.* 21:63. https://doi.org/10.1186/s12929-014-0063-5

Chi, L., A. Galtseva, L. Chen, R. Mo, C.C. Hui, and N.D. Rosenblum. 2013. Kif3a controls murine nephron number via GLI3 repressor, cell survival, and gene expression in a lineage-specific manner. *PLoS One.* 8:e65448. https://doi.org/10.1371/journal.pone.0065448

Coelho, P.A., L. Bury, M.N. Shahbazi, K. Liakath-Ali, P.H. Tate, S. Wormald, C.J. Hindley, M. Huch, J. Archer, W.C. Skarnes, et al. 2015. Over-expression of Plk4 induces centrosome amplification, loss of primary cilia and associated tissue hyperplasia in the mouse. *Open Biol.* 5:150209. https://doi.org/10.1098/rsob.150209

Cosenza, M.R., and A. Kramer. 2016. Centrosome amplification, chromosomal instability and cancer: mechanistic, clinical and therapeutic issues. *Chromosome Res.* 24:105–126.

Davenport, J.R., A.J. Watts, V.C. Roper, M.J. Croyle, T. van Groen, J.M. Wyss, T.R. Nagy, R.A. Kesterson, and B.K. Yoder. 2007. Disruption of intraflagellar transport in adult mice leads to obesity and slow-onset cystic kidney disease. *Curr. Biol.* 17:1586–1594. https://doi.org/10.1016/j.cub.2007.08.034

Dere, R., P.D. Wilson, R.N. Sandford, and C.L. Walker. 2010. Carboxy terminal tail of polycystin-1 regulates localization of TSC2 to repress mTOR. *PLoS One.* 5:e9239. https://doi.org/10.1371/journal.pone.0009239

Distefano, G., M. Boca, I. Rowe, C. Wodarczyk, L. Ma, K.B. Piontek, G.G. Germino, P.P. Pandolfi, and A. Boletta. 2009. Polycystin-1 regulates extracellular signal-regulated kinase-dependent phosphorylation of tuberin to control cell size through mTOR and its downstream effectors S6K and 4EBP1. *Mol. Cell. Biol.* 29:2359–2371. https://doi.org/10.1128/MCB.01259-08

Fisher, C.E., L. Michael, M.W. Barnett, and J.A. Davies. 2001. Erk MAP kinase regulates branching morphogenesis in the developing mouse kidney. *Development.* 128:4329–4338.

Ganem, N.J., S.A. Godinho, and D. Pellman. 2009. A mechanism linking extra centrosomes to chromosomal instability. *Nature.* 460:278–282. https://doi.org/10.1038/nature08136

Godinho, S.A., and D. Pellman. 2014. Causes and consequences of centrosome abnormalities in cancer. *Philos. Trans. R. Soc. Lond. B Biol. Sci.* 369:20130467. https://doi.org/10.1098/rstb.2013.0467

Godinho, S.A., M. Kwon, and D. Pellman. 2009. Centrosomes and cancer: how cancer cells divide with too many centrosomes. *Cancer Metastasis Rev.* 28:85–98. https://doi.org/10.1007/s10555-008-9163-6

Godinho, S.A., R. Picone, M. Burute, R. Dagher, Y. Su, C.T. Leung, K. Polyak, J.S. Brugge, M. Théry, and D. Pellman. 2014. Oncogene-like induction of cellular invasion from centrosome amplification. *Nature.* 510:167–171. https://doi.org/10.1038/nature13277

Goto, H., A. Inoko, and M. Inagaki. 2013. Cell cycle progression by the repression of primary cilia formation in proliferating cells. *Cell. Mol. Life Sci.* 70:3893–3905. https://doi.org/10.1007/s00018-013-1302-8

Habedanck, R., Y.-D. Stierhof, C.J. Wilkinson, and E.A. Nigg. 2005. The Polo kinase Plk4 functions in centriole duplication. *Nat. Cell Biol.* 7:1140–1146. https://doi.org/10.1038/ncb1320

Hartman, T.R., D. Liu, J.T. Zilfou, V. Robb, T. Morrison, T. Watnick, and E.P. Henske. 2009. The tuberous sclerosis proteins regulate formation of the primary cilium via a rapamycin-insensitive and polycystin 1-independent pathway. *Hum. Mol. Genet.* 18:151–163. https://doi.org/10.1093/hmg/ddn325

Hendry, C., B. Rumballe, K. Moritz, and M.H. Little. 2011. Defining and redefining the nephron progenitor population. *Pediatr. Nephrol.* 26:1395–1406. https://doi.org/10.1007/s00467-010-1750-4

Hoshi, M., J. Wang, S. Jain, and M.R. Mahjoub. 2015. Imaging centrosomes and cilia in the mouse kidney. *Methods Cell Biol.* 127:1–17. https://doi.org/10.1016/bs.mcb.2014.12.008

Jain, S. 2009. The many faces of RET dysfunction in kidney. *Organogenesis.* 5:177–190. https://doi.org/10.4161/org.5.4.10048

Jain, S., M. Encinas, E.M. Johnson Jr., and J. Milbrandt. 2006. Critical and distinct roles for key RET tyrosine docking sites in renal development. *Genes Dev.* 20:321–333. https://doi.org/10.1101/gad.1387206

Janssen, A., M. van der Burg, K. Szuhai, G.J. Kops, and R.H. Medema. 2011. Chromosome segregation errors as a cause of DNA damage and structural chromosome aberrations. *Science.* 333:1895–1898. https://doi.org/10.1126/science.1210214

Jonassen, J.A., J. San Agustin, J.A. Follit, and G.J. Pazour. 2008. Deletion of IFT20 in the mouse kidney causes misorientation of the mitotic spindle and cystic kidney disease. *J. Cell Biol.* 183:377–384. https://doi.org/10.1083/jcb.200808137

Keefe Davis, T., M. Hoshi, and S. Jain. 2013. Stage specific requirement of Gfrα1 in the ureteric epithelium during kidney development. *Mech. Dev.* 130:506–518. https://doi.org/10.1016/j.mod.2013.03.001

Kobayashi, A., M.T. Valerius, J.W. Mugford, T.J. Carroll, M. Self, G. Oliver, and A.P. McMahon. 2008. Six2 defines and regulates a multipotent self-renewing nephron progenitor population throughout mammalian kidney development. *Cell Stem Cell.* 3:169–181. https://doi.org/10.1016/j.stem.2008.05.020

Krämer, A., K. Neben, and A.D. Ho. 2005. Centrosome aberrations in hematological malignancies. *Cell Biol. Int.* 29:375–383. https://doi.org/10.1016/j.cellbi.2005.03.004

Kulukian, A., A.J. Holland, B. Vitre, S. Naik, D.W. Cleveland, and E. Fuchs. 2015. Epidermal development, growth control, and homeostasis in the face of centrosome amplification. *Proc. Natl. Acad. Sci. USA.* 112:E6311–E6320. https://doi.org/10.1073/pnas.1518376112

Levine, M.S., B. Bakker, B. Boeckx, J. Moyett, J. Lu, B. Vitre, D.C. Spierings, P.M. Lansdorp, D.W. Cleveland, D. Lambrechts, et al. 2017. Centrosome Amplification Is Sufficient to Promote Spontaneous Tumorigenesis in Mammals. *Dev. Cell.* 40:313–322.e5.

Lin, F., T. Hiesberger, K. Cordes, A.M. Sinclair, L.S. Goldstein, S. Somlo, and P. Igarashi. 2003. Kidney-specific inactivation of the KIF3A subunit of kinesin-II inhibits renal ciliogenesis and produces polycystic kidney disease. *Proc. Natl. Acad. Sci. USA.* 100:5286–5291. https://doi.org/10.1073/pnas.0836980100

Ma, M., A.R. Gallagher, and S. Somlo. 2017. Ciliary Mechanisms of Cyst Formation in Polycystic Kidney Disease. *Cold Spring Harb. Perspect. Biol.* 9:a028209. https://doi.org/10.1101/cshperspect.a028209

Mahjoub, M.R., and T. Stearns. 2012. Supernumerary centrosomes nucleate extra cilia and compromise primary cilium signaling. *Curr. Biol.* 22:1628–1634. https://doi.org/10.1016/j.cub.2012.06.057

Majumdar, A., S. Vainio, A. Kispert, J. McMahon, and A.P. McMahon. 2003. Wnt11 and Ret/Gdnf pathways cooperate in regulating ureteric branching during metanephric kidney development. *Development.* 130:3175–3185. https://doi.org/10.1242/dev.00520

Marthiens, V., M. Piel, and R. Basto. 2012. Never tear us apart--the importance of centrosome clustering. *J. Cell Sci.* 125:3281–3292. https://doi.org/10.1242/jcs.094797

Marthiens, V., M.A. Rujano, C. Pennetier, S. Tessier, P. Paul-Gilloteaux, and R. Basto. 2013. Centrosome amplification causes microcephaly. *Nat. Cell Biol.* 15:731–740. https://doi.org/10.1038/ncb2746

Masyuk, T.V., S.O. Lee, B.N. Radtke, A.J. Stroope, B. Huang, J.M. Banales, A.I. Masyuk, P.L. Splinter, S.A. Gradilone, G.B. Gajdos, and N.F. LaRusso. 2014. Centrosomal abnormalities characterize human and rodent cystic cholangiocytes and are associated with Cdc25A overexpression. *Am. J. Pathol.* 184:110–121. https://doi.org/10.1016/j.ajpath.2013.09.021

Mugford, J.W., J. Yu, A. Kobayashi, and A.P. McMahon. 2009. High-resolution gene expression analysis of the developing mouse kidney defines novel cellular compartments within the nephron progenitor population. *Dev. Biol.* 333:312–323. https://doi.org/10.1016/j.ydbio.2009.06.043

Mundlos, S., J. Pelletier, A. Darveau, M. Bachmann, A. Winterpacht, and B. Zabel. 1993. Nuclear localization of the protein encoded by the Wilms' tumor gene WT1 in embryonic and adult tissues. *Development.* 119:1329–1341.

Nano, M., and R. Basto. 2016. The Janus soul of centrosomes: a paradoxical role in disease? *Chromosome Res.* 24:127–144.

Nigg, E.A. 2006. Origins and consequences of centrosome aberrations in human cancers. *Int. J. Cancer.* 119:2717–2723. https://doi.org/10.1002/ijc.22245

Nigg, E.A., and T. Stearns. 2011. The centrosome cycle: Centriole biogenesis, duplication and inherent asymmetries. *Nat. Cell Biol.* 13:1154–1160. https://doi.org/10.1038/ncb2345

Ogden, A., P.C. Rida, and R. Aneja. 2013. Heading off with the herd: how cancer cells might maneuver supernumerary centrosomes for directional migration. *Cancer Metastasis Rev.* 32:269–287.

Patel, V., L. Li, P. Cobo-Stark, X. Shao, S. Somlo, F. Lin, and P. Igarashi. 2008. Acute kidney injury and aberrant planar cell polarity induce cyst formation in mice lacking renal cilia. *Hum. Mol. Genet.* 17:1578–1590. https://doi.org/10.1093/hmg/ddn045

Quintyne, N.J., J.E. Reing, D.R. Hoffelder, S.M. Gollin, and W.S. Saunders. 2005. Spindle multipolarity is prevented by centrosomal clustering. *Science.* 307:127–129. https://doi.org/10.1126/science.1104905

Roselli, S., O. Gribouval, N. Boute, M. Sich, F. Benessy, T. Attié, M.C. Gubler, and C. Antignac. 2002. Podocin localizes in the kidney to the slit diaphragm area. *Am. J. Pathol.* 160:131–139. https://doi.org/10.1016/S0002-9440(10)64357-X

Saifudeen, Z., S. Dipp, J. Stefkova, X. Yao, S. Lookabaugh, and S.S. El-Dahr. 2009. p53 regulates metanephric development. *J. Am. Soc. Nephrol.* 20:2328–2337. https://doi.org/10.1681/ASN.2008121224

Saifudeen, Z., J. Liu, S. Dipp, X. Yao, Y. Li, N. McLaughlin, K. Aboudehen, and S.S. El-Dahr. 2012. A p53-Pax2 pathway in kidney development: implications for nephrogenesis. *PLoS One.* 7:e44869. https://doi.org/10.1371/journal.pone.0044869

Schmidt-Ott, K.M., and J. Barasch. 2008. WNT/beta-catenin signaling in nephron progenitors and their epithelial progeny. *Kidney Int.* 74:1004–1008. https://doi.org/10.1038/ki.2008.322

Serçin, Ö., J.C. Larsimont, A.E. Karambelas, V. Marthiens, V. Moers, B. Boeckx, M. Le Mercier, D. Lambrechts, R. Basto, and C. Blanpain. 2016. Transient PLK4 overexpression accelerates tumorigenesis in p53-deficient epidermis. *Nat. Cell Biol.* 18:100–110. https://doi.org/10.1038/ncb3270

Shao, X., S. Somlo, and P. Igarashi. 2002. Epithelial-specific Cre/lox recombination in the developing kidney and genitourinary tract. *J. Am. Soc. Nephrol.* 13:1837–1846. https://doi.org/10.1097/01.ASN.0000016444.90348.50

Sharma, N., N.F. Berbari, and B.K. Yoder. 2008. Ciliary dysfunction in developmental abnormalities and diseases. *Curr. Top. Dev. Biol.* 85:371–427. https://doi.org/10.1016/S0070-2153(08)00813-2

Shillingford, J.M., N.S. Murcia, C.H. Larson, S.H. Low, R. Hedgepeth, N. Brown, C.A. Flask, A.C. Novick, D.A. Goldfarb, A. Kramer-Zucker, et al. 2006. The mTOR pathway is regulated by polycystin-1, and its inhibition reverses renal cystogenesis in polycystic kidney disease. *Proc. Natl. Acad. Sci. USA.* 103:5466–5471. https://doi.org/10.1073/pnas.0509694103

Silkworth, W.T., I.K. Nardi, L.M. Scholl, and D. Cimini. 2009. Multipolar spindle pole coalescence is a major source of kinetochore mis-attachment and chromosome mis-segregation in cancer cells. *PLoS One.* 4:e6564. https://doi.org/10.1371/journal.pone.0006564

Sillibourne, J.E., and M. Bornens. 2010. Polo-like kinase 4: the odd one out of the family. *Cell Div.* 5:25. https://doi.org/10.1186/1747-1028-5-25

Simons, M., J. Gloy, A. Ganner, A. Bullerkotte, M. Bashkurov, C. Krönig, B. Schermer, T. Benzing, O.A. Cabello, A. Jenny, et al. 2005. Inversin, the gene product mutated in nephronophthisis type II, functions as a molecular switch between Wnt signaling pathways. *Nat. Genet.* 37:537–543. https://doi.org/10.1038/ng1552

Srivastava, S., E. Molinari, S. Raman, and J.A. Sayer. 2018. Many Genes-One Disease? Genetics of Nephronophthisis (NPHP) and NPHP-Associated Disorders. *Front Pediatr.* 5:287. https://doi.org/10.3389/fped.2017.00287

Takakura, A., L. Contrino, X. Zhou, J.V. Bonventre, Y. Sun, B.D. Humphreys, and J. Zhou. 2009. Renal injury is a third hit promoting rapid development of adult polycystic kidney disease. *Hum. Mol. Genet.* 18:2523–2531. https://doi.org/10.1093/hmg/ddp147

Tammachote, R., C.J. Hommerding, R.M. Sinders, C.A. Miller, P.G. Czarnecki, A.C. Leightner, J.L. Salisbury, C.J. Ward, V.E. Torres, V.H. Gattone II, and P.C. Harris. 2009. Ciliary and centrosomal defects associated with mutation and depletion of the Meckel syndrome genes MKS1 and MKS3. *Hum. Mol. Genet.* 18:3311–3323. https://doi.org/10.1093/hmg/ddp272

Vitre, B., A.J. Holland, A. Kulukian, O. Shoshani, M. Hirai, Y. Wang, M. Maldonado, T. Cho, J. Boubaker, D.A. Swing, et al. 2015. Chronic centrosome amplification without tumorigenesis. *Proc. Natl. Acad. Sci. USA.* 112:E6321–E6330. https://doi.org/10.1073/pnas.1519388112

Werner, M.E., H.H. Ward, C.L. Phillips, C. Miller, V.H. Gattone II, and R.L. Bacallao. 2013. Inversin modulates the cortical actin network during mitosis. *Am. J. Physiol. Cell Physiol.* 305:C36–C47. https://doi.org/10.1152/ajpcell.00279.2012

Yoder, B.K. 2007. Role of primary cilia in the pathogenesis of polycystic kidney disease. *J. Am. Soc. Nephrol.* 18:1381–1388. https://doi.org/10.1681/ASN.2006111215

Zhao, H., H. Kegg, S. Grady, H.T. Truong, M.L. Robinson, M. Baum, and C.M. Bates. 2004. Role of fibroblast growth factor receptors 1 and 2 in the ureteric bud. *Dev. Biol.* 276:403–415. https://doi.org/10.1016/j.ydbio.2004.09.002